Conductive incubation and the origin of dome-and-keel structure in Archean granite-greenstone terrains: A model based on the eastern Pilbara Craton, Western Australia

Mike Sandiford

School of Earth Sciences, University of Melbourne, Melbourne, Victoria, Australia

Martin J. Van Kranendonk

Geological Survey of Western Australia, East Perth, Western Australia, Australia

Simon Bodorkos

School of Earth Sciences, University of Melbourne, Melbourne, Victoria, Australia

Received 24 August 2002; revised 28 August 2003; accepted 24 October 2003; published 27 January 2004.

[1] The Archean East Pilbara Granite-Greenstone Terrane (EPGGT) of the Pilbara Craton in Western Australia preserves a prolonged record of voluminous mafic-dominated volcanism and felsic plutonism, commencing at circa 3515 Ma and ultimately resulting in the development of spectacular ''dome-and-keel'' structures. Early crustal growth was dominated by basaltic magmatism and the regional development of a 12–18 km thick greenstone sequence by circa 3335 Ma, overlying widespread 3470–3430 Ma tonalite-trondhjemite-granodiorite (TTG) suites emplaced into the middle crust. Stratigraphic and structural relationships imply that voluminous granitoid plutonism and crustal-scale dome-and-keel formation in the southeastern EPGGT was not initiated until circa 3325 Ma but proceeded rapidly over the interval 3325–3308 Ma. This scenario is consistent with a ''conductive incubation'' period of 10–100 Myr duration, following the burial of radiogenic granitic crust beneath the accumulated greenstone pile. For heat production parameters appropriate to the 3515–3308 Ma EPGGT, we show that the burial of 3470–3430 Ma granitoid-rich crust beneath the $\geq$3335 Ma Euro Basalt and its precursors led to long-term crustal temperature increases of 170–234°C at 35 km depth, with a corresponding reduction in effective viscosity of 2–5 orders of magnitude. In combination with the greenstone-over-granitoid density inversion, the changes in effective viscosity of the mid to deep crust due to the burial of heat sources may have provided the crucial trigger for the initiation of dome-and-keel formation. Similarly, cooling and strengthening of the crust during syndoming exhumation of the heat production potentially terminated large-scale dome-and-keel amplification. *INDEX TERMS:* 8122 Tectonophysics: Dynamics, gravity and tectonics; 8130 Tectonophysics: Heat generation and transport; 8159 Tectonophysics: Rheology—crust and lithosphere; 8125 Tectonophysics: Evolution of the Earth; 9619 Information Related to Geologic Time: Precambrian; *KEYWORDS:* Archean, dome-and-keel structure, granite-greenstone terrains, Pilbara Craton. **Citation:** Sandiford, M., M. J. Van Kranendonk, and S. Bodorkos (2004), Conductive incubation and the origin of dome-and-keel structure in Archean granite-greenstone terrains: A model based on the eastern Pilbara Craton, Western Australia, *Tectonics*, *23*, TC1009, doi:10.1029/2002TC001452.

0278-7407/04/2002TC001452$12.00

1. Introduction

[2] Archean granite-greenstone terrains provide insight into the tectonic processes that built the oldest preserved continental crust, and thus represent a critical element in our understanding of the evolution of the Earth. The distinctive tectono-stratigraphic characteristic of many granite-greenstone terrains is a thick, dense supracrustal greenstone assemblage (dominated by mafic-ultramafic volcanic rocks) overlying a less dense and more evolved granitoid midcrust. Granitoid-dominated ''domes'' are usually exposed in the cores of antiformal culminations 30–120 km in diameter, and are separated by comparatively narrow, synclinal greenstone ''keels'' [e.g., *Eskola*, 1948; *MacGregor*, 1951; *Anhaeusser et al.*, 1969; *Hickman*, 1983, 1984; *Allen and Chamberlain*, 1989; *Marshak et al.*, 1992, 1997; *Choukroune et al.*, 1995; *Collins et al.*, 1998; *Van Kranendonk et al.*, 2002, 2004]. However, the fragmentary record of the Archean means that our understanding of the primary tectonic mechanisms responsible for early crustal growth and differentiation is incomplete [*Choukroune et al.*, 1997]. This record needs to be inferred from the geochemical fingerprints and structural geometries of the preserved crustal fragments, bearing in mind that the preservation process may well have been highly selective [*Morgan*, 1985].

[3] The large-scale development of ''dome-and-keel'' geometry is most prevalent in Archean and earliest Paleo-

proterozoic granite-greenstone terrains [*Marshak*, 1999, and references therein], the assembly and subsequent structural development of which has been the subject of extensive debate over the last 50 years [e.g., *MacGregor*, 1951; *Anhaeusser et al.*, 1969; *Burke et al.*, 1976; *Bickle et al.*, 1980; *Hickman*, 1984; *Kröner*, 1984; *Marshak et al.*, 1992; *Bouhallier et al.*, 1993; *Jelsma et al.*, 1993; *Choukroune et al.*, 1995; *Chardon et al.*, 1996, 2002; *Collins et al.*, 1998; *de Wit*, 1998; *Hamilton*, 1998; *Bleeker*, 2002]. With respect to the gross structural architecture of granite-greenstone terrains, two fundamental questions arise:

[4] 1. Is the greenstone-over-granite relationship a primary autochthonous feature of crustal growth, or is it related to allochthonous juxtaposition of discrete lithological packages?

[5] 2. Is the characteristic dome-and-keel geometry primarily due to ''vertical'' tectonic processes, such as ''partial convective overturn'' of the crust [e.g., *Collins et al.*, 1998] and/or diapirism [e.g., *Collins*, 1989; *Collins and Van Kranendonk*, 1999; *Van Kranendonk et al.*, 2002, 2004]; or ''horizontal'' interactions, such as thrusting followed by granitoid ascent within core complexes [e.g., *Zegers et al.*, 1996; *van Haaften and White*, 1998; *Kloppenburg et al.*, 2001]; or ''chocolate tablet'' extension [*Marshak*, 1999] resulting in granitoid domes within a network of broadly orthogonal-striking keels [*Blewett*, 2002]?

[6] It is crucial that any model for the evolution of Archean granite-greenstone terrains is based on an understanding of the mechanical behavior of the crustal materials involved. For example, with regard to the origin of dome-and-keel geometry, the widely observed superposition of thick, dense greenstones atop granitoid results in a crustal-scale gravitational instability. Such a density inversion provides an essential, but not necessarily sufficient, condition for the diapiric rise of granitoid rocks during partial convective overturn of the crust [e.g., *Mareschal and West*, 1980; *Collins et al.*, 1998]. In the Phanerozoic, density inversions of similar magnitude resulting from ophiolite obduction have rarely led to the generation of dome-and-keel structures [see *Davies and Warren*, 1988; *Hill et al.*, 1992, 1995]. Consequently, if dome-and-keel architecture in granite-greenstone terrains reflects gravitational instability, then the viscosity structure of Archean crust must have been rather different to that of Phanerozoic crust.

[7] In view of the fact that the effective viscosity of rocks depends on composition, stress and temperature [e.g., *Brace and Kohlstedt*, 1980; *Carter and Tsenn*, 1987; *Ranalli*, 1995], one potential reason for an unusual viscosity structure in granite-greenstone terrains relates to the distribution of radiogenic heat sources within Archean crust. It is widely appreciated that crustal thermal regimes are sensitive to the total abundance of radiogenic heat sources in the crust, with Mesoarchean heat production rates that were approximately 2–3 times modern day rates (depending on the concentrations of U, Th and K in the crust). However, it is less well understood that crustal thermal regimes are equally sensitive to the depth distribution of the heat production [*West and Mareschal*, 1979; *Mareschal and West*, 1980; *Ridley and Kramers*, 1990; *Parphenuk et al.*, 1994; *Chardon et al.*, 1998]. In the steady state conductive limit, the contribution of radiogenic heat sources to the temperature below the base of the heat-producing parts of the crust (T'_{qc}) can be expressed [e.g., *Sandiford and McLaren*, 2002] as

$$T'_{qc} = \frac{q_c h}{k} \tag{1}$$

where q_c is the depth-integrated heat production, h is the characteristic vertical length scale of the heat production distribution (see Appendix A), and k is the uniform, temperature-independent thermal conductivity. The significance of this simple relationship can easily be appreciated by considering the long-term thermal consequences of the emplacement of a 10 km thick greenstone succession (either autochthonous or allochthonous) atop a radiogenic crust with q_c = 60 mW m^{-2} (a value appropriate to granite-greenstone terrains in Archean times; see later discussion). The long-term increase in T'_{qc}(= $\Delta T'_{qc}$; see Appendix A) is given by

$$\Delta T'_{qc} = \frac{q_c h}{k} \tag{2}$$

[8] Assuming a bulk crustal k = 3 W m^{-1} °C^{-1} [e.g., *Haenel et al.*, 1988] and a burial-related Δh of 10 km, equation (2) yields a $\Delta T'_{qc}$ value of 200°C. We use the term ''conductive incubation'' to describe such long-term temperature increases, which are directly attributable to the deepening of granitoid-hosted radiogenic heat sources relative to the Earth's surface, and independent of concomitant changes in mantle heat flow. The physical mechanism of heating should not be confused with ''insulation'', which implies the existence of a thermal conductivity contrast between the granitoid substrate and the overlying greenstones. No such contrast is assumed in this study, despite the possibility that the bulk thermal conductivity of a ''real'' Archean supracrustal greenstone succession will be lower than that typical of the underlying granitoid rocks. Consequently, any potential increase in crustal temperatures resulting from such ''blanketing'' will be separate and additional to the thermal effects of conductive incubation that constitute the focus of this paper.

[9] As $\Delta T'_{qc}$ simply represents the long-term temperature change (at depths below the heat-producing parts of the crust) resulting from the vertical redistribution of heat sources, material points (such as the Moho) that undergo a change in depth as a consequence of this redistribution will be subject to additional temperature changes related to the ambient temperature gradient [*Sandiford and McLaren*, 2002]. For the Moho, the overall long-term change in temperature (ΔT_{Moho}) is approximated by

$$\Delta T_{\mathrm{Moho}} \approx \Delta T'_{qc} + \frac{q_m \Delta z_{\mathrm{Moho}}}{k} \tag{3}$$

where q_m is the mantle heat flow and (ΔT_{Moho}) is the change in Moho depth. It is therefore conceivable that dome-and-keel geometry in Archean granite-greenstone terrains is

related to an unusual viscosity regime in the mid to deep crust, driven by the thermal response of the crust to burial of radiogenic heat sources during emplacement of greenstones atop granitoids [*West and Mareschal*, 1979; *Mareschal and West*, 1980; *Ridley and Kramers*, 1990; *Parphenuk et al.*, 1994; *Chardon et al.*, 1998; *de Bremond d'Ars et al.*, 1999]. As noted above, the operation of such a mechanism implies a characteristic incubation period between greenstone emplacement and large-scale doming. The duration of this incubation will be comparable to the timescales typical of the conductive response of the crust to the vertical redistribution of radiogenic heat sources (i.e., $\geq$50 Myr).

[10] This paper reviews the evidence relating to primary crustal construction and subsequent dome-and-keel formation in the East Pilbara Granite-Greenstone Terrane (EPGGT; Figure 1a), with a view to testing the notion of conductive incubation as a potential driver for large-scale granite doming. Such an assessment relies on the critical analysis of structural and stratigraphic relationships at map scale (Figure 1a) [see also *Hickman and Lipple*, 1978], and the excellent exposure within the EPGGT makes it ideally suited to this purpose. Moreover, the availability (courtesy of Geoscience Australia) of high quality, calibrated airborne radiometric data (Figure 1b) for the EPGGT readily permits quantitative estimation of the spatial distribution of radiogenic heat sources [*Bodorkos et al.*, 2004]. While our prime focus is on the origin of the dome-and-keel geometry, we also review the evidence supporting autochthonous extrusion of the greenstone succession in an evolving crustal environment that also generated the granitoid components in the cores of the domes.

2. Regional Geological Framework

[11] The generation in the EPGGT of domal granitoid complexes 30–120 km in diameter punctuated a prolonged period of crustal growth spanning the interval >3515–2850 Ma [*Hickman*, 1983; *Buick et al.*, 1995; *Van Kranendonk et al.*, 2002], which was followed by eruption of the basalt-dominated Fortescue Group over the interval 2775–2630 Ma [*Arndt et al.*, 1991; *Wingate*, 1999; *Thorne and Trendall*, 2001]. *Nelson et al.* [1999] and *Van Kranendonk et al.* [2002] compiled the results of numerous U-Pb SHRIMP zircon studies and defined five major episodes of felsic magmatism. The widespread emplacement of voluminous 3490–3420 Ma tonalite-trondhjemite-granodiorite (TTG) rocks into the midcrust (mostly within the interval 3470–3430 Ma) was followed by granitoid intrusion and doming events at 3325–3308 Ma (in the eastern EPGGT), 3255–3235 Ma (in the north and west), and 2950–2930 Ma (along the western margin). Each of these episodes was bracketed by the eruption of voluminous mafic-ultramafic lavas and subordinate felsic volcanic rocks. Finally, posttectonic granite was emplaced into granitoid complexes throughout the EPGGT at circa 2850 Ma [*Hickman*, 1983; *Nelson*, 1998].

[12] Dome-and-keel structures are best developed in the area of the Mount Edgar and Corunna Downs granitoid complexes, and their surrounding greenstone belts in the southeastern EPGGT (Figure 1a) at circa 3325–3308 Ma [see *Collins*, 1989, 1993; *Williams and Collins*, 1990; *Collins et al.*, 1998; *Van Kranendonk et al.*, 2002]. In this area, felsic magmatism is dominated by 3325–3308 Ma rocks that comprise 75–90% of the Corunna Downs Granitoid Complex, over 50% of the Mount Edgar Granitoid Complex, and most of the felsic volcanic units in the greenstone belts flanking the Corunna Downs Granitoid Complex [*Van Kranendonk et al.*, 2001b]. The following section briefly summarizes the pre-3300 Ma geological development of the EPGGT, in order to provide a framework within which the sequence of events leading to the development of large-scale dome-and-keel structure may be understood.

[13] The Pilbara Supergroup comprises circa 3515–2940 Ma supracrustal greenstones [*Van Kranendonk et al.*, 2002, and references therein], and the basal (circa 3515–3426 Ma) part of the succession consists of three major, mafic volcanic-dominated packages (the Coonterunah Group, and the Talga Talga and Salgash Subgroups of the Warrawoona Group), each with a minimum thickness of several kilometers (Figure 2a) [see *Hickman*, 1983; *Van Kranendonk et al.*, 2002]. Contacts between successive greenstone packages are predominantly low strain, and vary from sharp angular unconformities [*Buick et al.*, 1995; *Van Kranendonk*, 2000], through low-angle disconformities to conformable contacts [*Hickman*, 1983]. Granitoid-greenstone interfaces are locally nonconformable [e.g., *Dawes et al.*, 1995] but most often display intrusive relationships, including contact metamorphic aureoles [*Van Kranendonk et al.*, 2002], even where the granitoid phase is only marginally younger than the overlying greenstones. Way-up indicators in the greenstone successions invariably define a radiating pattern, with younging directions away from the granitoid domes even in steeply dipping and locally overturned successions [*Van Kranendonk et al.*, 2001a, 2002], contradicting tectonic models proposing regional-scale thrust-related stacking and repetition of greenstone packages [e.g., *Bickle et al.*, 1980; *van Haaften and White*, 1998, 2001].

[14] Unless otherwise indicated, all dates cited in the following sections are weighted mean $^{207}Pb/^{206}Pb$ ages determined on zircon via SHRIMP, with errors quoted at 95% confidence.

2.1. Early Crust Formation (Circa 3515–3426 Ma)

[15] The oldest greenstone succession in the Pilbara Supergroup is the Coonterunah Group (Figure 1a). It ranges up to 6 km in thickness (Figure 2a) in the East Strelley greenstone belt [*Green et al.*, 2000] and is dominated by tholeiitic basalt interbedded with minor 3515 ± 3 Ma felsic volcanic rocks [*Buick et al.*, 1995]. A younger age limit for the Coonterunah Group is provided by a 3498 ± 2 Ma porphyritic rhyolite [*Nelson*, 2002] high in the sequence (Figures 2a and 2b).

[16] The second greenstone succession is the regionally extensive lowermost Warrawoona Group (Talga Talga Subgroup [see *Hickman*, 1983; *Van Kranendonk et al.*, 2002]), which has an average thickness of 8 km (ranging up to 10–12 km in the Marble Bar greenstone belt; Figure 2a). In the

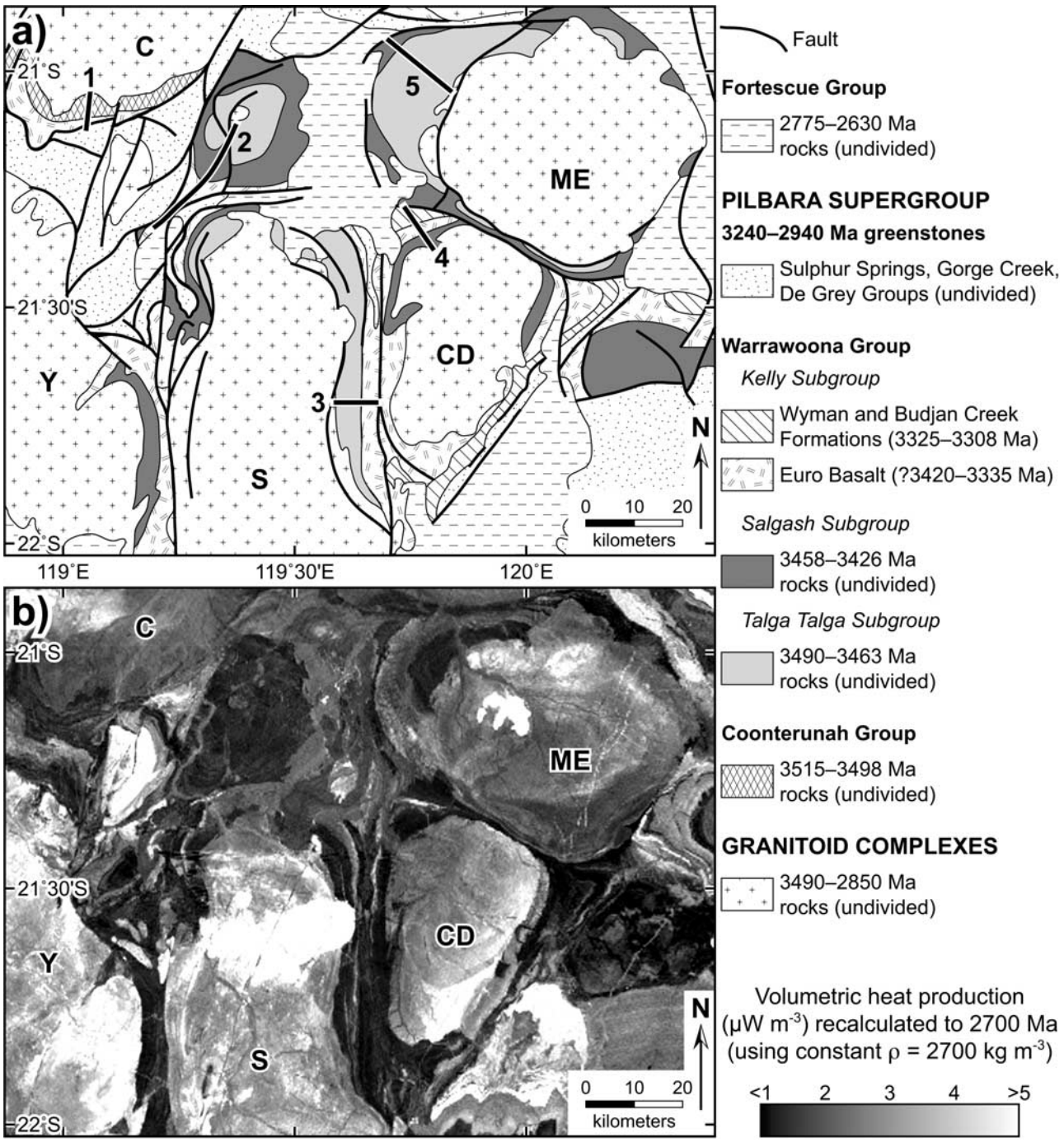

Figure 1. (a) Generalized geological map of the East Pilbara Granite-Greenstone Terrane (EPGGT), showing the locations (numbered heavy lines) of key stratigraphic sections within the lower Pilbara Supergroup from five greenstone belts (1, East Strelley; 2, Panorama; 3, Coongan; 4, Kelly (west); 5, Marble Bar; see Figure 2a). Names of granitoid complexes: C, Carlindie; CD, Corunna Downs; ME, Mount Edgar; S, Shaw; Y, Yule. (b) Volumetric heat production in the EPGGT (recalculated to 2700 Ma as the approximate time of cratonization) derived from the calibrated airborne radiometric data set acquired by Geoscience Australia.

Marble Bar greenstone belt, ultramafic rocks near the base of the Warrawoona Group were intruded by a retrogressed pyroxenite containing hornblende with a $^{40}Ar/^{39}Ar$ age of 3490 ± 15 Ma [*van Kooolwijk et al.*, 2001], and at a similar stratigraphic level in the Panorama greenstone belt (Figure 2a), a model Pb age of circa 3490 Ma was obtained on galena from a basalt-hosted syngenetic barite deposit [*Thorpe et al.*, 1992a]. Overlying basalts grade

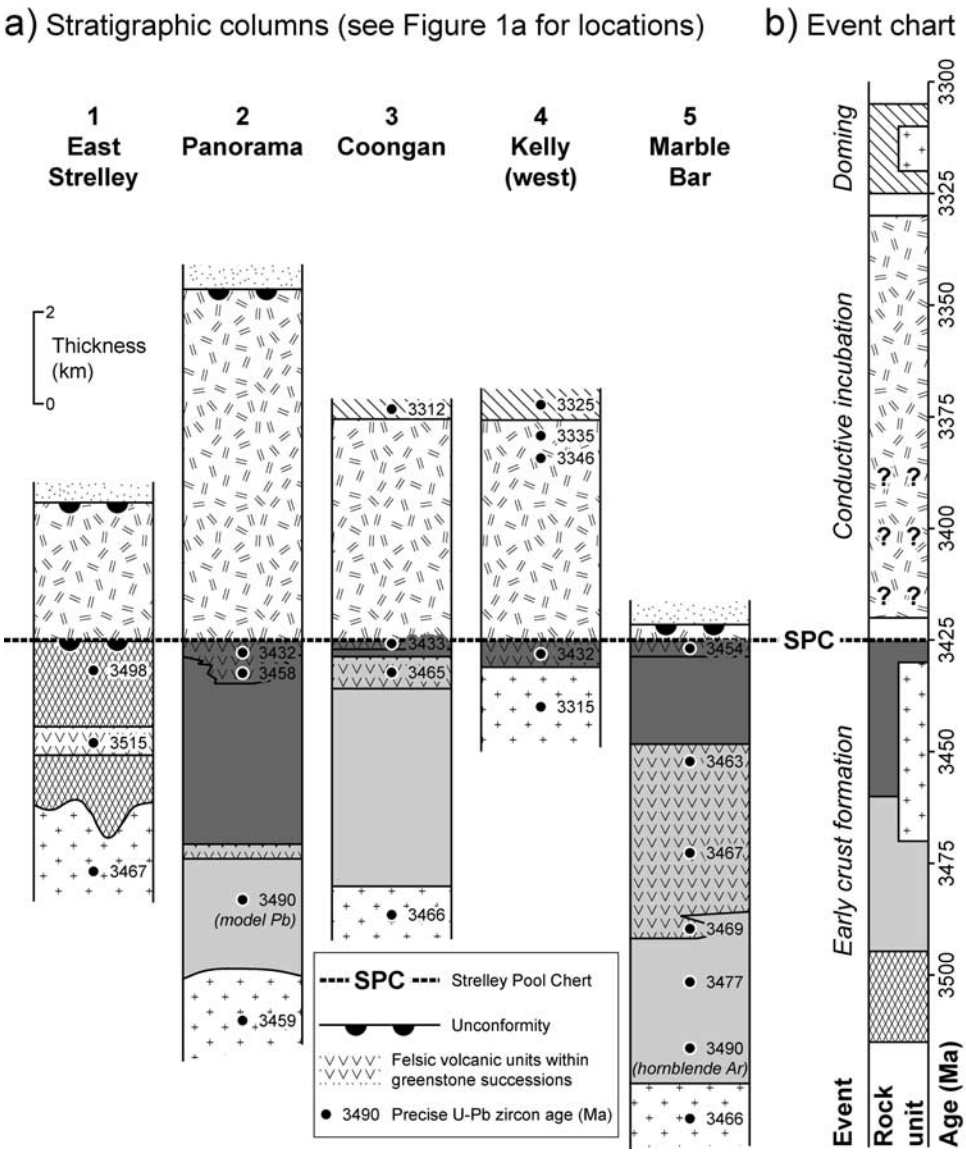

Figure 2. (a) Simplified stratigraphic sections 1–5 (see Figure 1a for locations) of pre-3300 Ma greenstones of the Pilbara Supergroup, ''hung'' to the volcanic hiatus represented by the regionally recognized, post-3426 Ma Strelley Pool Chert (SPC). Fill patterns for rock units are identical to those used in Figure 1a (''v'' pattern denotes felsic volcanic units within greenstone packages). Numbers within the sections indicate weighted mean U-Pb zircon ages (in Ma) with 2σ errors in the range ±2 Ma to ±7 Ma unless otherwise indicated. (b) Simplified event chart (also ''hung'' to the Strelley Pool Chert and with fill patterns for rock units identical to those used in Figure 1a) showing age ranges of the major greenstone successions and their relationships to major episodes of felsic plutonism. The age data define a three-stage geological evolution involving early crust formation (3515–3426 Ma), conductive incubation (?3420–3325 Ma), and granitoid doming (3325–3308 Ma).

into andesitic and rhyolitic rocks of the Duffer Formation, deposited over the interval 3474–3463 Ma [e.g., *Thorpe et al.*, 1992b; *McNaughton et al.*, 1993; *Nelson*, 1999, 2000, 2001]. Felsic volcanism was accompanied by voluminous TTG plutons (Figures 2b and 3a) emplaced into the lower parts of the greenstone successions [*Hickman*, 1983; *Bickle et al.*, 1993; *Collins*, 1993; *Smithies*, 2000; *Zegers and van Keken*, 2001]. Plutonic rocks coeval with the Duffer Formation dominate exposure in the Shaw Granitoid Complex [*Van Kranendonk*, 2000], and occur in significant volumes within the Mount Edgar and Carlindie granitoid complexes.

[17] The third pre-3426 Ma greenstone succession encompasses the midsection of the Warrawoona Group (Salgash Subgroup; redefined by *Van Kranendonk et al.* [2002] after *Hickman* [1983]), which attains an overall maximum thickness of 5 km in the Panorama greenstone

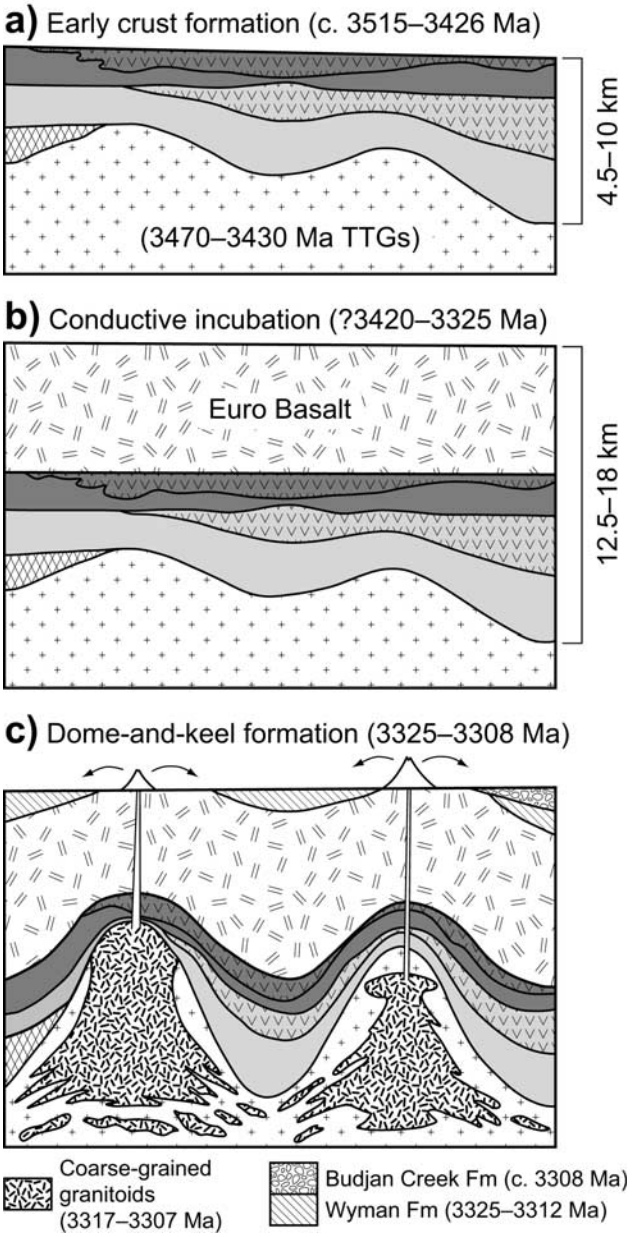

Figure 3. Schematic crustal sections showing the development of dome-and-keel geometry through time in the southeastern EPGGT (fill patterns are identical to those used in Figures 1a and 2a). (a) The earliest preserved crust in the EPGGT involved deposition of the Coonterunah Group and pre-3430 Ma greenstones of the Warrawoona Group and widespread emplacement of a 3470–3430 Ma TTG suite in the middle crust. (b) Deposition of the Euro Basalt prior to circa 3335 Ma amplified the density inversion and buried the radiogenic felsic crustal layer to depths of 12.5–18 km. (c) Large-scale dome-and-keel formation initiated at circa 3325 Ma. Voluminous 3317–3307 Ma granitoids of the Mount Edgar and Corunna Downs granitoid complexes were emplaced at high crustal levels relative to the surrounding greenstones, which sunk into the thermally weakened middle crust during 3325–3308 Ma deposition of felsic volcanic and volcaniclastic rocks.

belt (Figures 2a and 3a). The basal unit is the Apex Basalt, which is succeeded by 3458–3426 Ma felsic volcanic and volcaniclastic rocks of the Panorama Formation [e.g., *Thorpe et al.*, 1992b; *Nelson*, 2000, 2001, 2002]. In the Panorama greenstone belt (Figure 2a), emplacement of the small, shallow level North Pole Monzogranite laccolith (conventional U-Pb zircon age 3459 ± 18 Ma [*Thorpe et al.*, 1992b]) caused low-amplitude, syneruptive doming in coeval felsic volcaniclastic rocks [*DiMarco and Lowe*, 1989; *Van Kranendonk*, 2000].

2.2. Conductive Incubation (?3420–3325 Ma)

[18] Pre-3426 Ma volcanic rocks of the Coonterunah and Warrawoona Groups are overlain by the Strelley Pool Chert [*Lowe*, 1983; *Van Kranendonk and Morant*, 1998], a distinctive stromatolite-bearing unit of silicified quartzite and carbonate-chert laminites up to 30 m thick that has been recognized in greenstone belts across the entire EPGGT (Figures 2a and 2b). The 3458–3426 Ma felsic volcanic rocks underlying the Strelley Pool Chert provide a maximum depositional age; however, the unit accumulated during a period of regional volcanic quiescence and the age of cessation of deposition is not directly constrained (see section 3).

[19] The Strelley Pool Chert is overlain with apparent conformity by the Euro Basalt, which has depositional thicknesses in the range 4–9 km (Figures 2a and 3b) and comprises a basal succession (<3 km thick) of komatiite and high-Mg basalt that passes upward into tholeiitic basalt with frequent high-Mg basalt alternations [*Van Kranendonk*, 2000]. Critically, the maximum depositional age of the Euro Basalt remains poorly constrained (Figure 2b) due to a paucity of rock types suitable for dating; however, minimum ages for substantial accumulation of the Euro Basalt are over 80 Myr younger than the Strelley Pool Chert. Basalt-hosted felsic tuffs high in the succession contain dominant zircon populations at 3335 ± 7 Ma in the western Kelly greenstone belt [*Nelson*, 2003] and 3346 ± 6 Ma in the eastern Kelly greenstone belt [*Nelson*, 2001; *Van Kranendonk et al.*, 2002].

2.3. Doming of the Mount Edgar and Corunna Downs Granitoid Complexes (3325–3308 Ma)

[20] In greenstone belts flanking the Corunna Downs Granitoid Complex, a 500–1100 m thickness of rhyolites and volcaniclastic rocks of the 3325–3312 Ma Wyman Formation (Figure 3c) conformably to unconformably overlies the Euro Basalt [*Hickman*, 1983; *Pidgeon*, 1984; *Thorpe et al.*, 1992b; *McNaughton et al.*, 1993; *Barley et al.*, 1998; *Barley and Pickard*, 1999; *Nelson*, 2000, 2001, 2002; *Bagas*, 2003]. Voluminous felsic plutonism accompanied Wyman Formation deposition in the eastern EPGGT [*Williams and Collins*, 1990; *Barley and Pickard*, 1999; *Nelson*, 2000, 2001], with monzogranite and granodiorite generated over the interval 3317–3307 Ma (Figure 3c) comprising the dominant age component of the Corunna Downs and Mount Edgar granitoid complexes [*Barley and Pickard*, 1999; *Van Kranendonk et al.*, 2001b, 2002]. Geochemical studies suggest that these magmas were

derived via midcrustal to lower crustal partial melting of circa 3460 Ma TTG protoliths [*Collins*, 1989; *Bickle et al.*, 1993; *Barley and Pickard*, 1999].

[21] The initiation of dome-and-keel development in the southeastern EPGGT was synchronous with 3325–3308 Ma felsic magmatism, and is best illustrated by progressive tilting and folding of greenstones along the western, eastern and southern flanks of the Corunna Downs Granitoid Complex (Figure 4) [see also *Williams and Collins*, 1990; *Van Kranendonk et al.*, 2001b, 2002], and in the Warrawoona Syncline separating the Corunna Downs and Mount Edgar granitoid complexes [*Collins*, 1989; *Collins et al.*, 1998; *Collins and Van Kranendonk*, 1999]. South of the Corunna Downs Granitoid Complex (Figure 4), the Euro Basalt and Wyman Formation volcanic rocks with igneous crystallization ages of 3325 ± 4 Ma and 3323 ± 3 Ma [*Thorpe et al.*, 1992b; *McNaughton et al.*, 1993; *Nelson*, 2001] define a tight, east plunging syncline that is unconformably overlain by tilted but otherwise undeformed rocks of the 150–1200 m thick Budjan Creek Formation [*Van Kranendonk et al.*, 2001b; *Bagas and Van Kranendonk*, 2004]. This coarse-grained, rapidly accumulated volcaniclastic sedimentary unit hosts a crystal-lithic tuff with a zircon age of 3308 ± 5 Ma [*Nelson*, 2001; *Bagas and Van Kranendonk*, 2004], which represents a minimum age for the termination of syncline development in greenstone keels adjacent to the Corunna Downs Granitoid Complex [see *Collins et al.*, 1998].

[22] The notion that dome-and-keel formation near the Mount Edgar and Corunna Downs granitoid complexes was initiated before circa 3300 Ma conflicts with the regional structural synthesis of *Blewett* [2002], who suggested that substantial dome-and-keel development postdated deposition of banded iron formation of the <3240 Ma Gorge Creek Group, based on the existence of deep-seated magnetic anomalies that partially envelop granitoid complexes in parts of the EPGGT [e.g., *Wellman*, 2000]. However, the correlation of these anomalies with the lower Gorge Creek Group across the entire eastern Pilbara Craton is questionable, because even allowing for the obscuring effect of post-3240 Ma supracrustal rocks, the lateral extent and areal distribution of the magnetic anomalies far exceeds the surface exposure of the Gorge Creek Group (which is largely confined to the northern and western parts of the EPGGT). To the southeast, Gorge Creek Group exposure is limited to a single succession that unconformably overlies the 3308 ± 5 Ma Budjan Creek Formation (Figure 4) and therefore postdates syncline development in this area (see section 2.3).

[23] However, it should be noted that (1) major dome-and-keel development in parts of the northwestern EPGGT indisputably postdated deposition of the <3240 Ma Gorge Creek Group [*Blewett*, 2002; *Van Kranendonk et al.*, 2002] and (2) widespread (although relatively minor) episodic reactivation and amplification of dome-and-keel structure is recorded by supracrustal rocks as young as circa 2750 Ma throughout the EPGGT [e.g., *Thorne and Trendall*, 2001; *Van Kranendonk*, 2003]. It is conceivable that reactivation involved some degree of localized conductive incubation, possibly driven by periodic burial of granitoid-rich crust

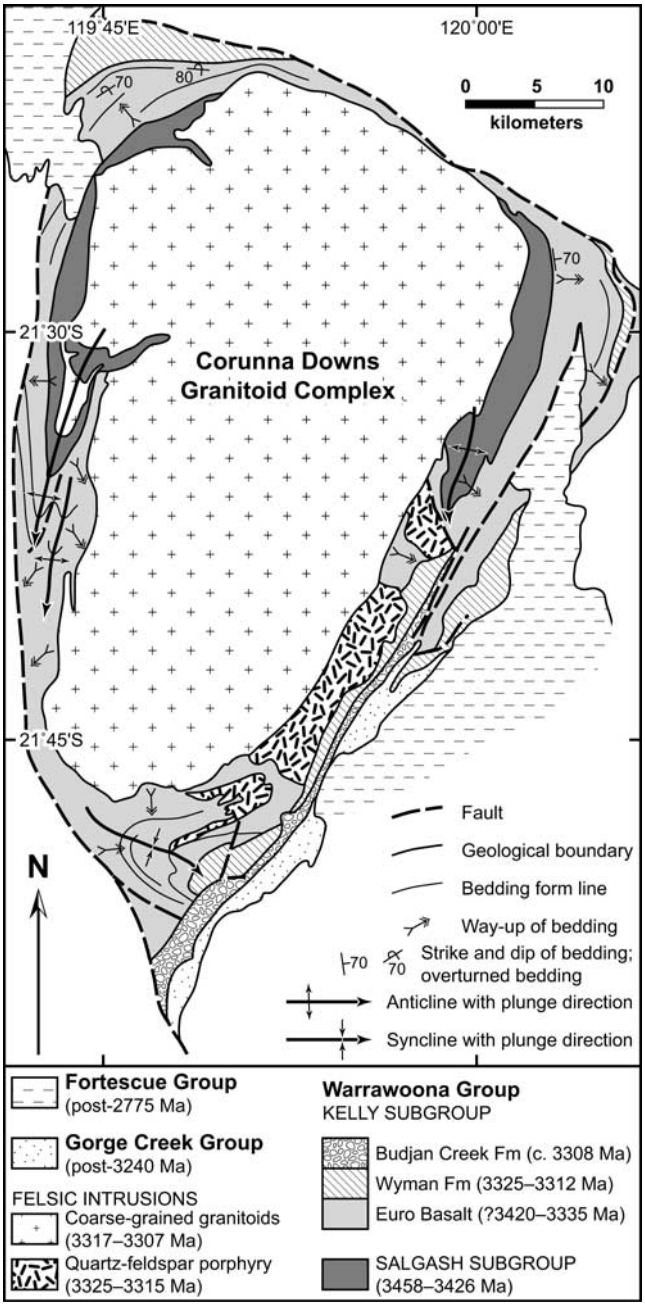

Figure 4. Simplified geological map of the Kelly greenstone belt and interpreted diapiric structures around the Corunna Downs Granitoid Complex (modified after *Van Kranendonk et al.* [2001b]). Note the hook-shaped folds on the western and eastern margins of the dome and the progressive development of the southernmost syncline, within which the pre-3335 Ma Euro Basalt and the 3325–3312 Ma Wyman Formation rocks are unconformably overlain by the tilted but otherwise undeformed circa 3308 Ma Budjan Creek Formation.

beneath greenstones of the upper Pilbara Supergroup (<3240–2750 Ma), and the overlying Fortescue Group (2775–2630 Ma).

3. Long-Term Thermal Consequences of Greenstone Emplacement

[24] As outlined in the introduction, the roles of "horizontal" and "vertical" tectonic processes in Archean dome-and-keel formation remains the subject of considerable debate, and it is beyond the scope of this paper to examine in detail the bodies of evidence supporting the various kinematic and structural models. Instead, we wish to emphasize the similarities between these models with respect to the first-order material transfer processes operating within the crust during dome-and-keel formation. Specifically, we aim to examine the long-term thermal evolution of a crust characterized by the emplacement (via thrusting or autochthonous eruption) of a thick greenstone edifice atop a less dense felsic substrate, followed by ascent of granitic rocks (via diapirism or extension-related core complex exhumation) relative to the overlying greenstones.

[25] The combination of an extended crustal prehistory (3515–3335 Ma), followed by rapid, large-scale granite plutonism and dome-and-keel development over the interval 3325–3308 Ma, is an important factor in the assessment of potential driving forces for granite dome formation and amplification. As noted in the introduction, the gross greenstone-over-granite architecture of the pre-3325 Ma EPGGT provides a necessary precondition for the initiation of partial convective overturn of the crust. However, the growth of any instability resulting from this inverted density stratification also requires an appropriate viscosity regime, which in turn is critically dependent on the thermal structure of the crust. In this respect, the accumulation of a thick greenstone edifice has two major consequences: (1) transient heat advection due to the ascent of voluminous mafic magmas such as the Euro Basalt and (2) a long-term heating of the crust via conductive incubation, due to the burial of radiogenic heat-producing elements beneath the accumulating greenstone pile.

[26] The extent of long-term midcrustal heating attributable to conductive incubation critically depends on the minimum age for substantial accumulation of the thick Euro Basalt (section 2.2, Figure 3b). Unfortunately, the duration of the volcanic hiatus that accompanied deposition of the underlying post-3426 Ma Strelley Pool Chert is unconstrained, and it is conceivable that very slow accumulation of this 30-m-thick unit (over several tens of Myr) was followed by eruption of the entire 4–9 km thickness of the Euro Basalt over the interval circa 3350–3325 Ma. Alternatively, it is possible that relatively rapid accumulation of the Strelley Pool Chert (within a few Myr) was immediately followed by eruption of the komatiitic lower Euro Basalt as early as circa 3410 Ma [*Van Kranendonk et al.*, 2001b], and subsequent paraconformable deposition of the 3346–3335 Ma upper Euro sequence (section 2.2).

[27] In any case, dome-and-keel development at 3325–3308 Ma postdated substantial deposition of the Euro Basalt by at least 10 Myr, and possibly by as much as 100 Myr. This implies that transient heating associated with the syneruptive passage of Euro basaltic magmas through the crust did not provide the primary trigger for dome-and-keel formation. We therefore turn our attention to the potential role of conductive incubation, by estimating the magnitude of long term burial-related crustal heating using the available constraints on the overall abundance (q_c) and vertical distribution (h) of radiogenic heat-producing elements in the southeastern EPGGT at circa 3300 Ma.

[28] The value of q_c at 3300 Ma may be estimated from modern measurements of surface heat flow and surface heat production rates, because primary crustal growth in the vicinity of the Mount Edgar and Corunna Downs granitoid complexes was substantially complete by this time. The present-day surface heat flow in the EPGGT is ~45 mW m^{-2} [*Cull*, 1982], a value typical of Archean cratons worldwide [*Vitorello and Pollack*, 1980; *Nyblade and Pollack*, 1993]. This value represents the cumulative contribution of (1) predominantly crust-hosted radiogenic heat sources and (2) heat flux related mainly to convection in the sublithospheric mantle.

[29] An upper limit on the deep mantle contribution to surface heat flow (q_m) is approximated by the average thermal gradient prevailing in the lithosphere in the absence of crustal radiogenic heat sources, i.e.,

$$q_m = k\frac{\Delta T_L}{\Delta z_L} \tag{4}$$

where ΔT_L is the present-day temperature difference between the Earth's surface and the base of the conductive lithosphere (i.e., $\Delta T_L = 1250–1300$°C), and Δz_L is the present-day thickness of the lithosphere. The results of seismic refraction studies suggest that Δz_L is 250–300 km in the EPGGT [*Drummond*, 1988], and assigning a temperature-independent bulk thermal conductivity k = 3 W m^{-1} °C^{-1}, the present-day mantle heat flow contribution q_m is estimated at 12–18 mW m^{-2} using equation (4) [see *Jaupart and Mareschal*, 1999]. By difference from the surface heat flow value, the likely range of possible values for the total radiogenic heat production contribution q_c is of the order 25–35 mW m^{-2}. Heat production rates at 3300 Ma were approximately 2.4 times greater than modern day rates for the U, Th and K contents representative of EPGGT granites (Table 1), which implies that q_c at 3300 Ma was in the range 60–85 mW m^{-2}.

4. Conductive Incubation: A Model and Its Results

[30] In the introduction, we showed that the burial of a radiogenic crust (q_c = 60 mW m^{-2}) beneath a greenstone succession 10 km thick produced a significant long-term temperature increase ($\Delta T'_{qc}$ = 200°C) at depths below the heat-producing part of the crust. We now present the results of a finite element model simulating the thermal evolution of the EPGGT, which solves the one-dimensional, time-dependent heat flow equation in a moving medium. The

Table 1. Average K, Th, U, and Heat Production Rates for the Major Pre-3300 Ma Granitoid Complexes in the Southeastern EPGGT[a]

Granitoid Complex	Area,[b] %	K, wt %	Th, ppm	U, ppm	Heat Production,[c] μW m^{-3}	
					Present-Day	3300 Ma
Mount Edgar (n = 212)[d]	37	2.7 ± 1.4	16.7 ± 11.6	2.4 ± 2.7	2.2 ± 1.5	4.8 ± 3.2
Corunna Downs (n = 209)	22	3.7 ± 1.2	13.5 ± 7.6	2.5 ± 1.5	1.9 ± 0.9	4.8 ± 1.9
Shaw (n = 19)[e]	41	3.7 ± 1.4	24.6 ± 14.4	2.6 ± 1.2	2.6 ± 1.3	5.6 ± 2.2

[a]Data from Geoscience Australia's OZCHEM database. Uncertainties represent one standard deviation.
[b]Calculated using Figure 1b, with the area of pre-3300 Ma granite exposure in the Mount Edgar, Corunna Downs, and Shaw granitoid complexes normalized to 100%.
[c]Assuming a uniform granite density of 2700 kg m^{-3}.
[d]Excludes the high heat-producing circa 2850 Ma Moolyella Monzogranite.
[e]Excludes the high heat-producing circa 2850 Ma Cooglegong Monzogranite.

general form of the equation [e.g., *Turcotte and Schubert*, 1982] is

$$\rho c\left(\frac{\partial T}{\partial t}+U\frac{\partial T}{\partial z}\right)=k\frac{\partial^2 T}{dz^2}+H \qquad (5)$$

where ρ is density, c is heat capacity, U is the vertical velocity (positive downward) of the reference frame (i.e., $U = \partial z/\partial t$), and H is the radiogenic heat production in the system.

4.1. Initial Conditions

[31] We define t = 0 at 3515 Ma, and consider a differentiated initial crust comprising a 12 km thick granitoid layer (within which radiogenic heat sources are uniformly distributed), overlying a depleted lower crust with negligible heat production that is indistinguishable (in terms of its thermal properties) from lithospheric mantle material. Using the constraints on q_c from section 3, two limiting cases are considered: q_c = 85 mW m^{-2} and q_c = 60 mW m^{-2} (equivalent to uniform heat production H values of 7.1 and 5.0 μW m^{-3}, respectively, within the 12 km thick granitoid layer; see Table 1). In both cases, the depth distribution of the heat production corresponds to an initial characteristic vertical length scale (h) of 6 km (equation (A8); see also *Sandiford et al.* [2002] and *Sandiford and McLaren* [2002]).

[32] For a uniform, constant thermal conductivity k = 3 W m^{-1} °C^{-1}, the steady state (t = 0) radiogenic crustal contribution to the geotherm (T'_{qc}) below the base of the granitoid layer (i.e., for $z \geq$ 12 km) is 170°C for q_c = 85 mW m^{-2}, and 120°C for q_c = 60 mW m^{-2} (equation (A9)). For a specified value of q_m, the initial temperature field $T(z, 0)$ is defined by equations (A5a)–(A5c), with h_1 = 0 km, $h_2 - h_1$ = 12 km, H_1 = 0 μW m^{-3}, and H_2 = 7 μW m^{-3} (for q_c = 85 mW m^{-2}) or H_2 = 5 μW m^{-3} (for q_c = 60 mW m^{-2}).

4.2. Solution of the Time-Dependent Heat Flow Equation for a Specific Geological History

[33] We now consider the solution of equation (5) and the thermal evolution of the one-dimensional crustal system in response to a specific history of greenstone accumulation and subsequent granitoid doming, based on the geological data presented in section 2 (see Table 2). The model greenstones comprise four discrete successions, each with a vertical thickness Δh that accumulated at a uniform rate over a specified age range Δt (Table 2). In combination, these properties define the time-dependent (but discontinuous) vertical velocity U of the reference frame (U = 0 outside the age ranges specified in Table 2).

[34] Note that within the available age constraints, we have assumed relatively slow accumulation and a young age for the Euro Basalt (Table 2). This conservative assumption minimizes the time interval available for thermal relaxation of the crust following completion of the model greenstone edifice (at 3340 Ma) but prior to the initiation of dome-and-keel formation (at 3325 Ma), thereby ensuring that the temperature increases due to conductive incubation predicted by the model represent minimum estimates. One-dimensional dome-and-keel formation is

Table 2. Model History of Greenstone Deposition and Granite Doming in the Eastern EPGGT[a]

Greenstone Deposition or Granite Doming Event	Burial/Ascent Δh, km	Age Range Δt, Ma	Vertical Velocity $U = \Delta h/\Delta t$, km Myr^{-1}
Coonterunah Group	+2	3515–3495	0.10
Lower Warrawoona (Talga Talga Subgroup)	+3	3490–3465	0.12
Middle Warrawoona (Salgash Subgroup)	+2	3460–3430	0.07
Euro Basalt	+7	3380–3340	0.18
Ascent of the Mount Edgar and Corunna Downs granitoid complexes	−10	3325–3308	−0.59

[a]Implemented as a series of changes in h (at a uniform rate over specified time intervals) that are separated by periods of quiescence. In Figures 5–7 a shaded zone represents each event.

implemented as an exhumation of heat production to shallower crustal levels (i.e., negative Δh), during ascent and emplacement of 3325–3308 Ma granitoids (Table 2).

[35] Figure 5a illustrates the model history of greenstone deposition and granitoid doming listed in Table 2. Figures 5b and 5c show the attendant changes in temperature attributable to conductive incubation (ΔT_{qc}) at depths of 20, 30, 40, and 50 km, for q_c = 85 mW m^{-2} (Figure 5b) and q_c = 60 mW m^{-2} (Figure 5c). Note that the specified depths are time-invariant, so the curves of ΔT_{qc} versus time do not represent the thermal histories of material points (which change depth during burial and subsequent exhumation). Figure 6 shows the time-dependent change in ΔT_{qc} as a function of depth at critical stages in the model history, corresponding to the initiation and cessation of each greenstone accumulation episode, the initiation and cessation of dome-and-keel formation, and thermal relaxation of the postdoming configuration.

[36] The four-stage accumulation of the greenstone sequence atop the felsic crust results in an overall increase in h of 14 km (h = 20 km at 3340 Ma; Figure 5a). If this configuration is permitted to reach thermal equilibrium, equation (2) estimates the long-term temperature increase at and below the base of the heat–producing layer (relative to the initial crust) in the range $\Delta T'_{qc}$ = 280–397°C for q_c = 60–85 mW m^{-2}. However, thermal equilibration of the predoming crust is precluded by the relatively short interval (15 Myr) between the cessation of Euro Basalt accumulation and the initiation of granitoid ascent (Table 2). Therefore, in order to assess the extent of partial thermal relaxation experienced by the midcrust to deep crust prior to dome-and-keel-formation, we define the parameter $T_{qc(35\ km)}$ as the radiogenic component of the temperature field at 35 km depth, and consider its time-dependent variation.

[37] Accumulation of the first three greenstone successions results in $T_{qc(35\ km)}$ increasing from 120–170°C (at 3515 Ma) to 186–259°C (at 3430 Ma), corresponding to the range q_c = 60–85 mW m^{-2} (Figure 7a). Following cessation of Euro Basalt eruption at 3340 Ma and subsequent thermal relaxation, $T_{qc(35\ km)}$ = 290–404°C at 3325 Ma (Figure 7a). This corresponds to $\Delta T_{qc(35\ km)}$ = 170–234°C relative to the initial configuration, i.e., approximately 60% of the completely equilibrated value ($\Delta T'_{qc}$ = 280–397°C) predicted by equation (2). At 3325 Ma, the initiation of dome-and-keel formation, and shallowing of the heat-producing layer to half its predoming depth (i.e., Δh = 10 km, Table 2), immediately triggers rapid cooling in the middle and lower crust. By circa 3275 Ma, $T_{qc(35\ km)}$ values are approximately 60–100 °C below their 3325 Ma peak (Figure 7a).

[38] Importantly, the curves of $T_{qc(35\ km)}$ versus time in Figure 7a assume that all of the pre-3300 Ma heat production was present at 3515 Ma. However, detailed geochemical studies of the widespread 3470–3430 Ma TTG suite in the EPGGT suggest that the magmas were derived via high-pressure partial melting of eclogite [e.g., *Bickle et al.*, 1993; *Collins*, 1993; *Smithies*, 2000] and it is possible that this differentiation event was responsible for large-scale addition of radiogenic heat production to the crust. Figures 7b and 7c show thermal evolutions analogous to Figure 7a, corresponding to scenarios where only 50% and 30% (respectively) of the total budget of heat-producing elements (q_c) was resident in the crust at 3515 Ma, with the remainder being added to the granitoid layer at a uniform rate over the interval 3470–3430 Ma. In both cases, initial $T_{qc(35\ km)}$ values are very low in proportion to the reduced values of q_c at 3515 Ma (equation (1)), and early (pre-3430 Ma) conductive incubation and heating is similarly subdued. However, once the full complement of heat production is present in the crust at 3430 Ma, progressive thermal equilibration over the ensuing 100 Myr prior to doming ensures that the peak $T_{qc(35\ km)}$ values attained at 3325 Ma (270–380°C and 263–371°C in Figures 7b and 7c, respectively) are not significantly different from the scenario considered in Figure 7a.

[39] Comparing the model results to the thermal evolution of the EPGGT is subject to some important limitations. In addition to the fact that temperature evolutions were calculated for depth-invariant points, we have neglected the role of thermal transients associated with autochthonous extrusion of the greenstone successions, the magnitude and spatial patterning of which will have been determined largely by the character of the magma plumbing systems that fed the eruption centers. Consequently, the curves depicted in Figures 5–7 cannot easily be equated with material points in the EPGGT crust.

[40] Nevertheless, Figures 5–7 highlight the fact that burial of a radiogenic granitoid layer beneath a thick greenstone succession must have led to long-term heating of the order of hundreds of degrees at mid to deep crustal levels in the EPGGT. This heating occurred on timescales appropriate to the characteristic conductive response time of the lithosphere ($\geq$50 Myr), and therefore outlasted thermal transients associated with greenstone emplacement. In addition, the progressive burial of material points (such as the Moho) during greenstone accumulation subjected those points to additional temperature increases over and above those indicated in Figures 5–7 (see equation (3)). The magnitude of this temperature increase is largely controlled by the mantle heat flow (q_m), and the occurrence in the EPGGT of voluminous, predominantly basaltic 3515–3340 Ma volcanic rocks suggests that contemporary q_m was relatively high [see *Richter*, 1985; *Bickle*, 1986; *Vlaar et al.*, 1993; *Abbott et al.*, 1994]. For q_m = 40 mW m^{-2} and k = 3 W m^{-1} °C^{-1}, the second term on the right-hand side of equation (3) predicts that burying the Moho by the accumulated thickness of the greenstone pile (i.e., $\Delta z_{Moho} = \Delta h$ = 14 km) will increase the Moho temperature (ΔT_{Moho}) by 187°C, independent of the thermal effects of conductive incubation. When the concomitant increase in $T_{qc(35\ km)}$ is taken into account (e.g., $\Delta T_{qc(35\ km)}$ = 170–234°C at 3325 Ma relative to the 3515 Ma crust, Figure 7a), equation (3) raises the possibility that the overall temperature increase experienced by the Moho as a consequence of thick greenstone accumulation atop a highly radiogenic Archean felsic crust may be as high as 350–420°C.

[41] The impact of such a temperature change will be profound in terms of both the evolution of the Moho and

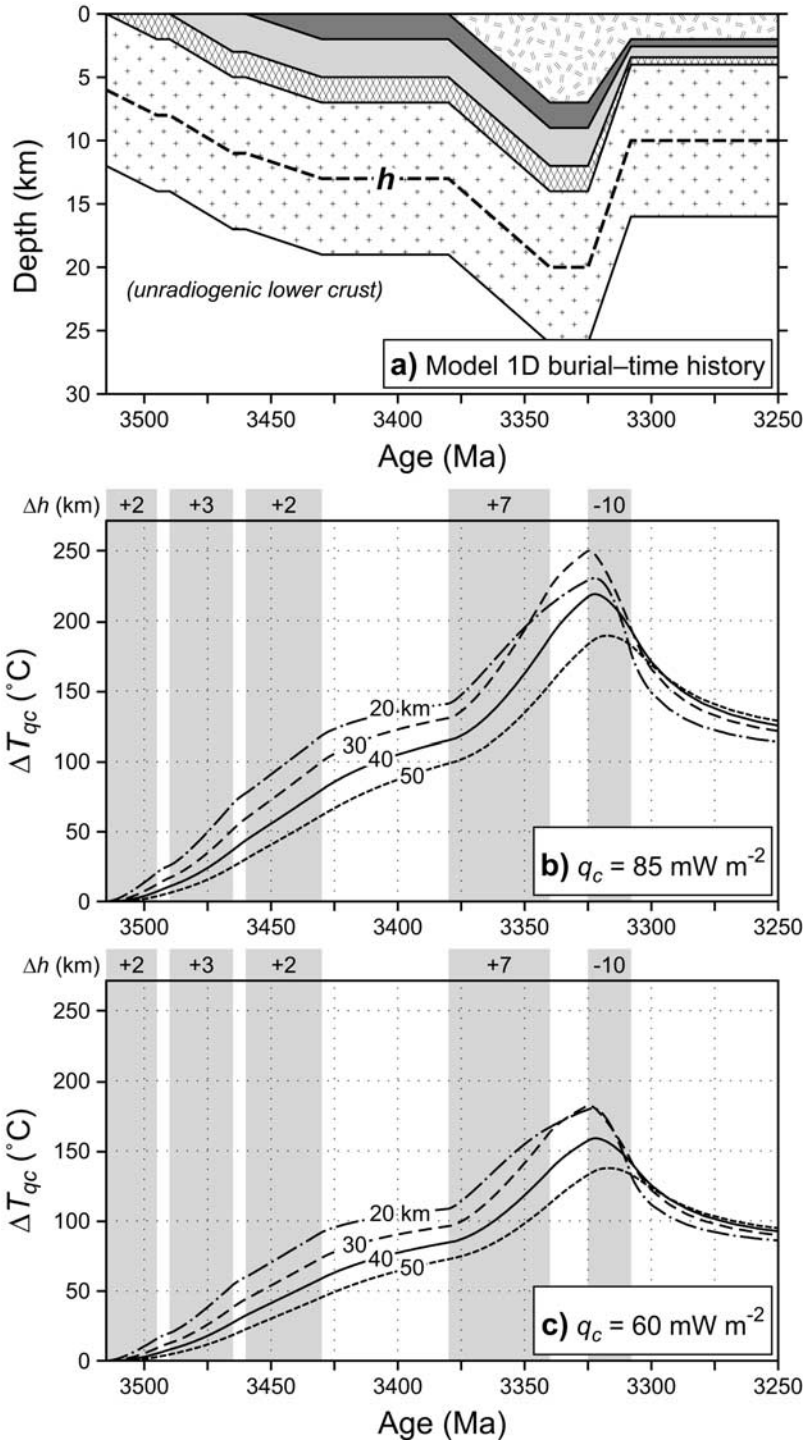

Figure 5. (a) Burial time plot, showing the model evolution of the one-dimensional rock column summarized in Table 2 (fill patterns for rock units are identical to those used in Figure 1a). The heavy dashed line labeled "*h*" shows the time-dependent variation of the characteristic depth of the heat production. (b) Calculated temperature changes (ΔT_{qc}) over the interval 3515–3250 Ma at time-invariant depths 20, 30, 40, and 50 km (relative to the surface) due to episodic changes in *h* (shaded gray) during the history of greenstone accumulation and subsequent dome-and-keel formation shown in Figure 5a, for $q_c = 85$ mW m^{-2}. (c) As for Figure 5b, with $q_c = 60$ mW m^{-2}. Note that individual curves in Figures 5b and 5c track ΔT_{qc} at constant depths and do not represent material points (which change depth as they are buried and exhumed).

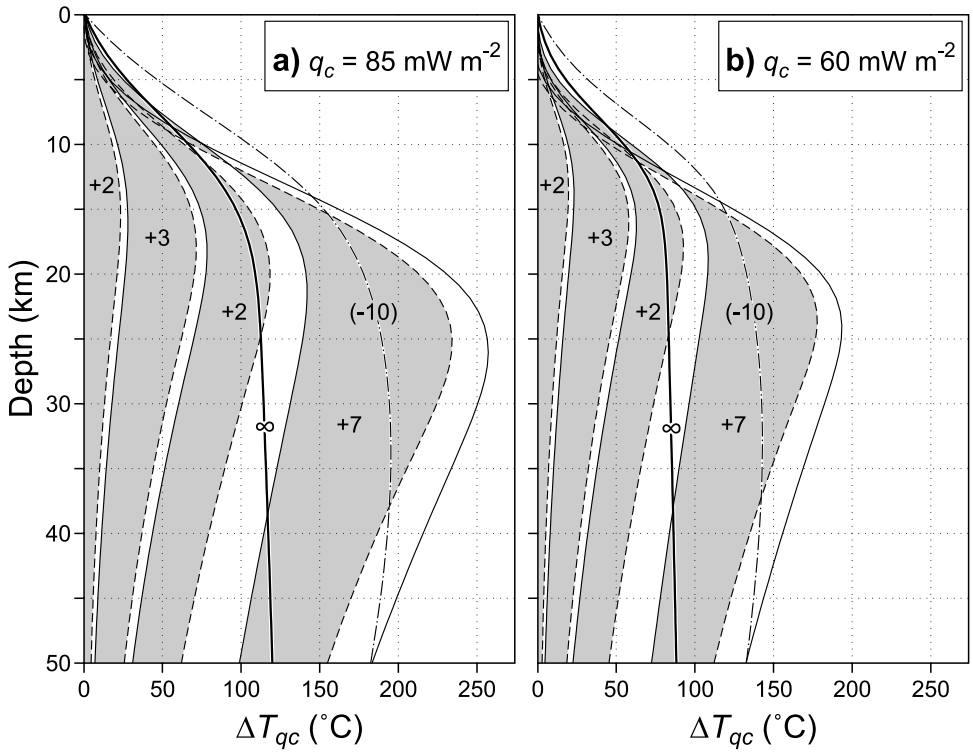

Figure 6. Changes in ΔT_{qc} through time as a function of depth for (a) q_c = 85 mW m^{-2} and (b) q_c = 60 mW m^{-2}. Shaded areas with numerical labels correspond to the Δh events (values in km) defined in Figure 5a and Table 2. ΔT_{qc} is shown at the start (solid lines) and finish (dashed lines) of each depositional episode, immediately prior to doming (thin black line, no shading); at the cessation of doming (dot-dashed line labeled " − 10") and following complete thermal relaxation of the postdoming crustal configuration (heavy black line labeled "∞").

lower crust (discussed in more detail in section 5), and the viscosity structure of the midcrust. In the context of dome-and-keel formation, one simple way to investigate the temperature dependence of viscosity is to consider the stress regime prevailing during buoyancy-driven ascent of a relatively low-density granitoid dome into a denser, overlying greenstone carapace. The effective stress (σ) is of the order $\Delta\rho gr$, where $\Delta\rho$ is the greenstone-granite density contrast, g is gravitational acceleration, and r is the radius of the dome [*Weinberg and Podladchikov*, 1994]. The effective viscosity μ_{eff} is of the order

$$\mu_{\text{eff}} \approx \frac{\sigma}{\dot{\varepsilon}} \approx \frac{\sigma}{Ae^{-E/RT}\sigma^n} \frac{1}{Ae^{-E/RT}(\Delta\rho gr)^{n-1}} \tag{6}$$

where R is the universal gas constant and A, E, and n are material constants governing creep rates of the rock. The decrease in the viscosity of the midcrust to lower crust in response to any temperature increase ΔT may then be expressed in terms of a ratio that eliminates several of the material constants, i.e.,

$$\frac{\mu_{\text{eff}}(T+\Delta T)}{\mu_{\text{eff}}(T)} = \frac{A(\Delta\rho gr)^{n-1}e^{-E/RT}}{A(\Delta\rho gr)^{n-1}e^{-E/RT(T+\Delta T)}} \tag{7}$$

which reduces to

$$\ln\left[\frac{\mu_{\text{eff}}(T+\Delta T)}{\mu_{\text{eff}}(T)}\right] = \frac{E}{R}\left(\frac{1}{T} - \frac{1}{T+\Delta T}\right) \tag{8}$$

[42] Therefore the magnitude of the viscosity decrease at a specified depth depends on the initial temperature (T), the magnitude of the temperature increase (ΔT) due to conductive incubation, and the activation energy (E) of the crustal material involved. For the specific properties and geological history of the one-dimensional rock column modeled in Figures 5–7 (i.e., k = 3 W m^{-1}°C^{-1}, and h effectively independent of q_c due to the absence of heat production outside a granitoid layer of time-invariant thickness), the initial (3515 Ma) temperature at 35 km depth $T_{(35\text{ km})}$ is a linear function of q_m and q_c (see equations (A5c) and (A9)). For q_m = 30, 40, and 50 mW m^{-2} (Figures 8a–8c, respectively) at 3515 Ma, Figure 8 (left) shows the range of $T_{(35\text{ km})}$ values in terms of q_c values applicable to the Archean EPGGT. As each model assumes a time-invariant q_m, ΔT is entirely attributable to conductive incubation, and Figure 7a shows that relative to $T_{qc(35\text{ km})}$ at 3515 Ma, $\Delta T_{qc(35\text{ km})}$ = 170–234°C at 3325 Ma (for q_c = 60–85 mW m^{-2}; see Figure 8, left).

[43] With the temperature parameters constrained, the magnitude of the viscosity decrease depends only on the

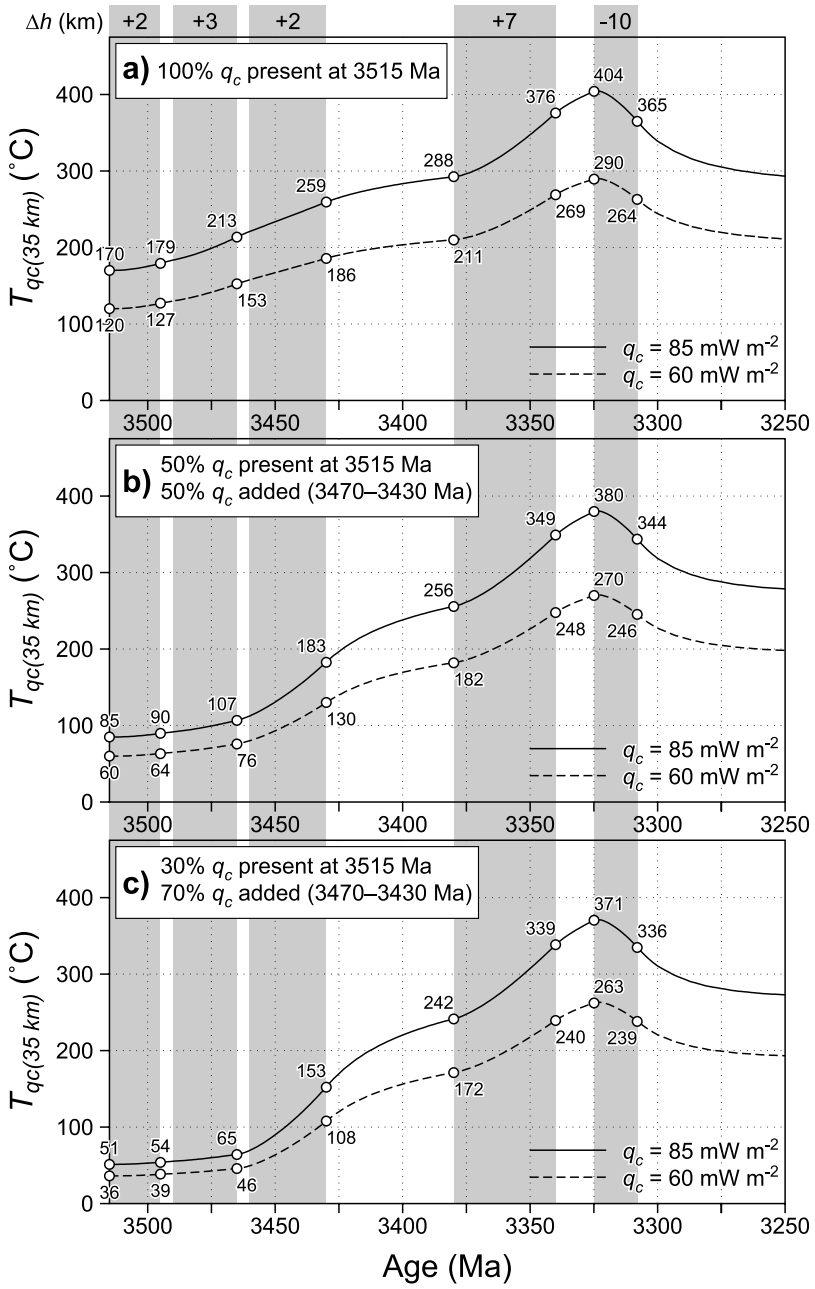

Figure 7. Evolution of the mean temperature component at 35 km depth ($T_{qc(35\ km)}$) attributable to radiogenic heating as a function of the event history defined in Figure 5a and Table 2, for $q_c = 85$ mW m^{-2} and $q_c = 60$ mW m^{-2}. Figures 7a, 7b, and 7c differ only in the assumed history of q_c addition to the crust (see text for discussion). Numbers represent the values of $T_{qc(35\ km)}$ at critical points in the evolution.

activation energy E, and Figure 8 (right) shows that quartz-rich felsic crust ($E \sim 140$–180 kJ mol^{-1}; Figure 8) will undergo a reduction of effective viscosity of 2–5 orders of magnitude, depending primarily on the initial thermal structure of the crust. Note that the lowest viscosity contrasts (Figure 8c) are likely to represent minimum estimates, as they correspond to very high $T_{(35\ km)}$ values. It is likely that such elevated temperatures ($T \geq 800$°C [see *Collins et al.*, 1998]) will trigger widespread partial melting within the buried granitoid layer, further decreasing the effective viscosity of the midcrust, but our models do not consider this effect.

5. Discussion and Conclusions

[44] One of the most important changes in the geochemical structure of the crust between the Archean and the present-day has been the secular decline in radiogenic heat

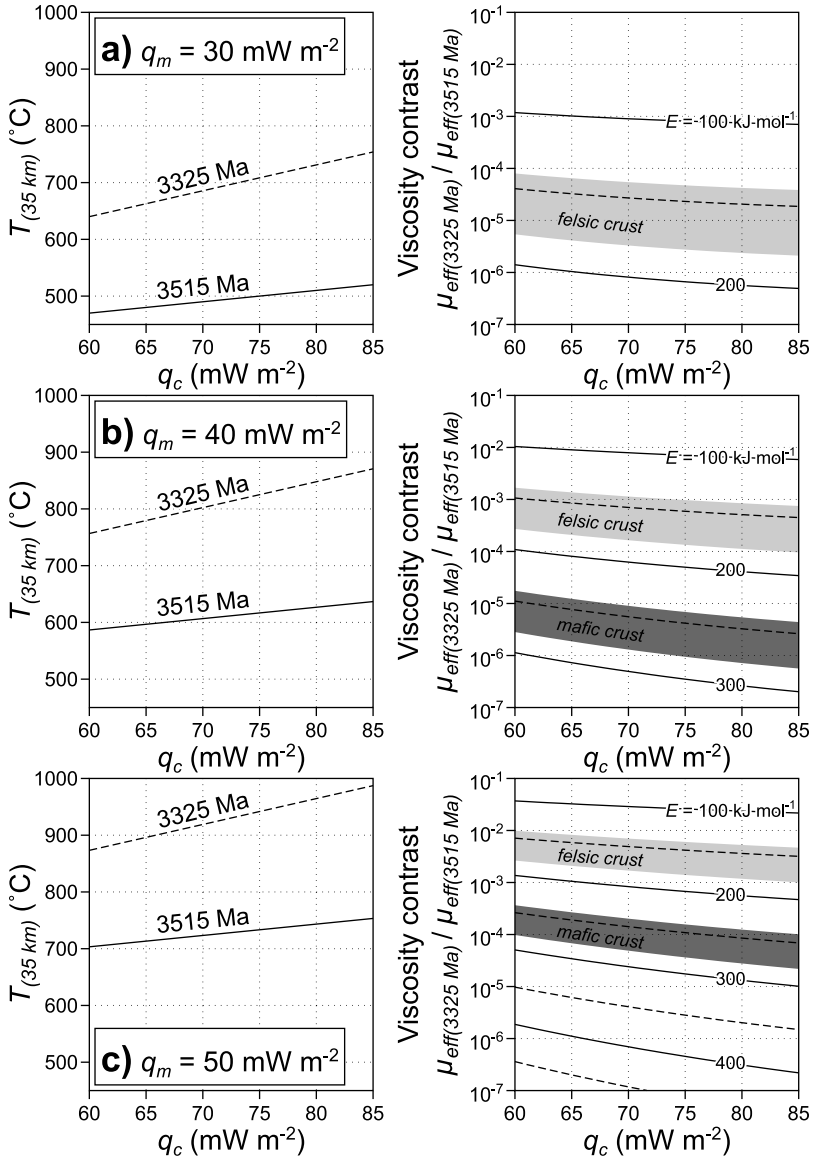

Figure 8. (left) Contributions of q_m and q_c to the total temperature field at 35 km depth ($T_{(35\ km)}$) for the initial crustal configuration (3515 Ma) and that immediately prior to the commencement of dome-and-keel formation (3325 Ma). Figures 8a, 8b, and 8c differ only in the (constant) value of q_m assumed. (right) Relationship between the effective viscosity ratio (defined in equation (8), with $\mu_{eff}(T)$ calculated using $T_{(35\ km)}$ at 3515 Ma, and $\mu_{eff}(T + \Delta T)$ calculated using $T_{(35\ km)}$ at 3325 Ma) and q_c for a range of activation energies (E) typical of felsic and mafic crust (data sources are *Shelton and Tullis* [1981], *Hansen and Carter* [1982], *Kirby* [1983], and *Kirby and Kronenberg* [1984]). The temperature increases implied by our model results for the EPGGT at 35 km depth suggest that the effective viscosity of the quartz-rich granitoid midcrust is reduced by 2–5 orders of magnitude between the initiation of greenstone deposition and the commencement of dome-and-keel formation. The magnitude of the effective viscosity decrease depends principally on the magnitudes of q_m and q_c, which determine the $T_{(35\ km)}$ value of the initial configuration.

production. For example, data constraining present-day heat flow and lithosphere thickness in the EPGGT imply that radiogenic heat production contributed at least 60 mW m^{-2} to the surface heat flow at circa 3300 Ma, 50–100% more than the mean contribution of 30–40 mW m^{-2} in modern day continents [*McLennan and Taylor*, 1996]. However, while the importance of the total abundance of heat-producing elements in deciphering Archean crustal and tectonic processes has long been recognized, the impact of the depth distribution of heat production has not been clearly understood [e.g., *West and Mareschal*, 1979; *Mareschal and West*, 1980; *England and Bickle*, 1984].

[45] Equation (1) shows that changing the characteristic vertical length scale of the heat production (h) is just as important for crustal thermal regimes as changing the total abundance of heat-producing elements (q_c) [see *Sandiford et al.*, 2002; *Sandiford and McLaren*, 2002]. Thus for q_c values appropriate to the mid-Archean EPGGT, the burial of heat-producing granitoid crust during greenstone accumulation yields dramatic increases in midcrustal to deep crustal temperatures, and corresponding reductions in crustal viscosity. For the greenstone accumulation history considered here, the implied temperature increases at 35 km depth average between 170 and 234°C prior to dome-and-keel formation, with resultant reductions in effective viscosity of the order 10^2–10^5. In the EPGGT, the accumulation of the thick Euro Basalt was of crucial importance because it led to a long term, burial-related temperature increase of ~90–120°C in the mid to deep crust (Figure 7a). The fact that this heating outlived Euro volcanism is consistent with the notion that conductive incubation was an essential precursor for large-scale dome-and-keel formation.

[46] The large reductions in the long-term effective viscosity of the mid to lower crust raise important concerns about its mechanical stability. The inherent weakness of such crust implies that it should be very sensitive to even moderate levels of imposed tectonic stress. To the extent that any deformation is likely to produce topography on preexisting density interfaces within the lithosphere, the calculations summarized here suggest that for the thermal regimes appropriate to the Archean crust with a thick carapace of greenstone, the buoyancy arising from such interfaces is likely to have been effective at amplifying unstable perturbations (or dampening stable perturbations). In the case of the EPGGT, ascent of granitoid rocks during dome-and-keel formation resulted in the large-scale transfer of heat-producing elements to shallower crustal levels, leading to long-term cooling of the mid to deep crust and thereby increasing its effective viscosity and mechanical strength. Cooling and strengthening of the middle and upper crust following dome-and-keel formation was further enhanced by geochemical fractionation directly related to magmatism, with the Yule, Shaw, and Mount Edgar granitoid complexes all containing late stage, high-level intrusions that display strong K, Th and U enrichment (Figure 1b; and see *Hickman* [1983], *Champion and Smithies* [2000], and *Bodorkos et al.* [2004]).

[47] The analysis of the long term thermal consequences of greenstone emplacement presented here provides a potential basis for understanding the role of internal buoyancy in creating the crustal architecture preserved in the EPGGT and other dome-and-keel terrains. However, it is important to recognize that the mechanical behavior of the upper crust is unlikely to resemble that of a viscous fluid, even if pervasively serpentinized ultramafic rocks control its bulk rheology [e.g., *de Bremond d'Ars et al.*, 1999]. The brittle strength of the upper crust will exert significant control on the extent of partial convective overturn of the inverted density profile, and it is likely that a secondary process such as significant lateral extension is necessary to weaken and/or rupture the brittle upper crust before large-scale dome-and-keel formation can proceed [e.g., *Bleeker*, 2002]. In this context, the extreme heating experienced by the material Moho as a result of the combined effects of burial and conductive incubation (ΔT_{Moho} = 350–420°C, see section 4.2) is especially relevant, as significant lateral flow of the hot lower crust (and shallowing of the Moho via crustal-scale extension) represents the most viable mechanism for the reestablishment of thermal equilibrium.

[48] Finally, the model espoused here does not militate against any particular hypothesis for the origin of the "primary" tectono-stratigraphic assembly (whereby a layer of dense, unradiogenic rock is emplaced above a less dense layer enriched in heat-producing elements). Such an arrangement could conceivably result from allochthonous processes and large-scale tectonic duplication of the crust in settings analogous to modern convergent plate boundaries or, as *Hickman* [1983, 1984] and *Van Kranendonk et al.* [2002] have argued for the EPGGT, from the autochthonous extrusion of basaltic edifices atop preexisting felsic crust.

[49] With regard to this problem, our most important insight is that the final dome-and-keel architecture retains little memory of the processes responsible for the initiating configuration. Rather, this characteristic geometry represents a "structural reorganization" essential to stabilize both the viscosity and the density distribution of the Archean crust. One consequence of the secular decline in radiogenic crustal heat production is that orogenic systems have become progressively less prone to this type of reorganization, and more likely to preserve directly the structures associated with orogenic construction. Whereas orogenic systems in the modern Earth are strongly forced by plate interactions (and preserve a long-term memory of this forcing), the inherent thermal and mechanical properties of Archean crust ensured that the preserved record of "primary" plate interactions, orogeny and crustal assembly is relatively fragmentary.

Appendix A: Steady State Geotherm in a Two-Layer Crust and Its Dependence on the Depth Distribution of Heat Production

A1. General Analytic Expression for the Steady State Geotherm in a Two-Layer Stratified Crust

[50] We solve the one-dimensional heat flow equation for a simple "two-layer" vertical distribution of radiogenic heat sources. Consider a crust (with surface temperature T_s, uniform and temperature-independent thermal conductivity k) comprising an upper layer (depth $0 \le z \le h_1$) and a lower layer (depth $h_1 \le z \le h_2$) with homogeneous volumetric heat productions H_1 and H_2, respectively. For depth $z \ge h_2$, the abundance of heat-producing elements is negligible, and the mantle heat flow is denoted q_m. The energy conservation equation states

$$k\frac{d^2T}{dz^2} + H_1 = 0 \qquad 0 \le z \le h_1 \qquad \text{(A1a)}$$

$$k\frac{d^2T}{dz^2} + H_2 = 0 \qquad h_1 \le z \le h_2 \qquad \text{(A1b)}$$

$$k\frac{d^2T}{dz^2} = 0 \qquad z > h_2 \qquad \text{(A1c)}$$

At the layer interfaces, Fourier's law of heat conduction takes the form

$$-q(z=0) = k\frac{dT}{dz} = q_m + h_1(H_1 - H_2) + h_2H_2 \qquad 0 \le z \le h_1 \qquad \text{(A2a)}$$

$$-q(z=h_1) = k\frac{dT}{dz} = q_m - h_1H_2 + h_2H_2 \qquad h_1 \le z \le h_2 \qquad \text{(A2b)}$$

$$-q(z=h_2) = k\frac{dT}{dz} = q_m \qquad z > h_2 \qquad \text{(A2c)}$$

The negative sign on the left-hand side is due to upward directed heat flow in a crust with z defined as positive downward. Integrating (A1a)–(A1c) with respect to z, applying (A2a)–(A2c) as the respective boundary conditions and rearranging yields

$$\frac{dT}{dz} = \frac{1}{k}[q_m + h_1(H_1 - H_2) + h_2H_2 - H_1z] \qquad 0 \le z \le h_1 \qquad \text{(A3a)}$$

$$\frac{dT}{dz} = \frac{1}{k}(q_m + h_2H_2 - H_2z) \qquad h_1 \le z \le h_2 \qquad \text{(A3b)}$$

$$\frac{dT}{dz} = \frac{q_m}{k} \qquad z > h_2 \qquad \text{(A3c)}$$

Integrating equation (A3a) with respect to z and applying the boundary condition $T(z = 0) = T_s$:

$$T(z) = \frac{1}{k}\left\{T_s + [q_m + h_1(H_1 - H_2) + h_2H_2]z - \frac{H_1}{2}z^2\right\} \qquad 0 \le z \le h_1 \qquad \text{(A4a)}$$

Integrating equation (A3b) with respect to z and applying the boundary condition $T(z = h_1) = T(h_1)$ derived from equation (A4a):

$$T(z) = \frac{1}{k}\left[T_s + \frac{h_1^2(H_1 - H_2)}{2} + (q_m + h_2H_2)z - \frac{H_2}{2}z^2\right] \qquad h_1 \le z \le h_2 \qquad \text{(A4b)}$$

Integrating equation (A3c) with respect to z and applying the boundary condition $T(z = h_2) = T(h_2)$ derived from equation (A4b):

$$T(z) = \frac{1}{k}\left[T_s + \frac{h_1^2(H_1 - H_2) + h_2^2H_2}{2} + q_mz\right] \qquad z > h_2 \qquad \text{(A4c)}$$

Equations (A4a)–(A4c) define the piecewise-continuous steady state geotherm.

A2. Relationships Between T'_{qc}, q_c, and h

[51] In this paper, we consider the special case in which a granitoid layer with uniform heat production H_2 and thickness $(h_2 - h_1)$ is buried beneath a greenstone layer with thickness h_1 and negligible heat production (i.e., $H_1 = 0$). Assuming $T_s = 0°C$, equations (A4a)–(A4c) reduce to

$$T(z) = \frac{q_m}{k}z + \frac{H_2(h_2 - h_1)}{k}z \qquad 0 \le z \le h_1 \qquad \text{(A5a)}$$

$$T(z) = \frac{q_m}{k}z + \frac{H_2}{k}\left(h_2 - \frac{z}{2}\right)z - \frac{H_2h_1^2}{2k} \qquad h_1 \le z \le h_2 \qquad \text{(A5b)}$$

$$T(z) = \frac{q_m}{k}z + \frac{H_2\left(h_2^2 - h_1^2\right)}{2k} \qquad z > h_2 \qquad \text{(A5c)}$$

The first term on the right-hand side of equations (A5a)–(A5c) represents the component of the temperature field due to the heat flow from beneath the heat-producing section of the lithosphere (i.e., the mantle heat flow), which is denoted T_{qm}. The other terms on the right hand side of equations (A5a)–(A5c) represent the contribution to the temperature field due to radiogenic heat sources in the crust, defined as T_{qc}. The maximum value of T_{qc} (denoted T'_{qc}) is attained at the depth below which the abundance of heat-producing elements is negligible (i.e., $z > h_2$ in this case). From equation (A5c),

$$T'_{qc} = \frac{H_2\left(h_2^2 - h_1^2\right)}{2k} \qquad \text{(A6)}$$

Equation (A6) can be reexpressed in terms of the depth-integrated heat production q_c (i.e., the radiogenic crustal contribution to surface heat flow) and the characteristic vertical length scale h of the heat production distribution. In this case, q_c is given by

$$q_c = \int_{h_1}^{h_2} H_2dz = H_2(h_2 - h_1) \qquad \text{(A7)}$$

and h is defined as the depth midpoint of the heat-producing granitoid layer:

$$h = h_1 + \frac{h_2 - h_1}{2} = \frac{h_2 + h_1}{2} \qquad \text{(A8)}$$

Substituting (A7) and (A8) into (A6) gives

$$T'_{qc} = \frac{q_ch}{k} \qquad \text{(A9)}$$

The magnitude of the long-term change in T'_{qc} (i.e., $\Delta T'_{qc}$) accompanying the burial (positive Δh) or exhumation

(negative Δh) of a heat-producing granitoid layer is given by

$$T'_{qc} + \Delta T'_{qc} = \frac{q_c(h + \Delta h)}{k} \quad \text{(A10)}$$

assuming that the thickness of the granitoid layer is maintained. So

$$\Delta T'_{qc} = \frac{q_c \Delta h}{k} \quad \text{(A11)}$$

Thus for fixed q_c and k, $\Delta T'_{qc}$ depends only on Δh and is independent of the initial h value.

[52] **Acknowledgments.** We thank Richard Blewett and David Champion (Geoscience Australia) for providing access to the East Pilbara airborne radiometric data set (Figure 1b) and the OZCHEM geochemical database (Table 1), respectively, and Arthur Hickman and Ian Tyler (Geological Survey of Western Australia) for their comments on an earlier version of the manuscript. Journal reviewers Wouter Bleeker and Stephen Marshak and Associate Editor David Evans are thanked for thorough, constructive, and insightful reviews that considerably improved the focus and clarity of the material presented. Martin Van Kranendonk publishes with the permission of the Director of the Geological Survey of Western Australia.

References

Abbott, D., L. Burgess, and J. Longhi (1994), An empirical thermal history of the Earth's upper mantle, *J. Geophys. Res.*, *99*, 13,835–13,850.

Allen, T., and C. P. Chamberlain (1989), Thermal consequences of mantled gneiss dome emplacement, *Earth Planet. Sci. Lett.*, *93*, 392–404.

Anhaeusser, C. R., R. Mason, M. J. Viljoen, and R. P. Viljoen (1969), A reappraisal of some aspects of Precambrian shield geology, *Geol. Soc. Am. Bull.*, *80*, 2175–2200.

Arndt, N. T., D. R. Nelson, W. Compston, A. F. Trendall, and A. M. Thorne (1991), The age of the Fortescue Group, Hamersley Basin, Western Australia, from ion microprobe zircon U-Pb results, *Aust. J. Earth Sci.*, *38*, 261–281.

Bagas, L. (2003), Stratigraphic revision of the Warrawoona and Gorge Creek Groups in the Kelly greenstone belt, Pilbara Craton, Western Australia, in *Geological Survey of Western Australia Annual Review 2001/02*, pp. 53–60, Geol. Surv. of West. Aust., Perth.

Bagas, L., and M. J. Van Kranendonk (2004), Geology of the Split Rock 1:100,000 sheet, 1:100,000 geological series explanatory notes, Geol. Surv. of West. Aust., Perth, in press.

Barley, M. E., and A. L. Pickard (1999), An extensive, crustally derived, 3325 to 3310 Ma silicic volcanoplutonic suite in the eastern Pilbara Craton: Evidence from the Kelly Belt, McPhee Dome, and Corunna Downs Batholith, *Precambrian Res.*, *96*, 41–62.

Barley, M. E., S. E. Loader, and N. J. McNaughton (1998), 3430 to 3417 Ma calc-alkaline volcanism in the McPhee Dome and Kelley Belt, and growth of the eastern Pilbara Craton, *Precambrian Res.*, *88*, 3–24.

Bickle, M. J. (1986), Implications of melting for stabilisation of the lithosphere and heat loss in the Archaean, *Earth Planet. Sci. Lett.*, *80*, 314–324.

Bickle, M. J., L. F. Bettenay, C. A. Boulter, D. I. Groves, and P. Morant (1980), Horizontal tectonic interaction of an Archaean gneiss belt and greenstones, Pilbara Block, Western Australia, *Geology*, *8*, 525–529.

Bickle, M. J., L. F. Bettenay, H. J. Chapman, D. I. Groves, N. J. McNaughton, I. H. Campbell, and J. R.de Laeter (1993), Origin of the 3500–3300 Ma calc-alkaline rocks in the Pilbara Archaean: Isotopic and geochemical constraints from the Shaw Batholith, *Precambrian Res.*, *60*, 117–149.

Bleeker, W. (2002), Archaean tectonics: A review, with illustrations from the Slave Craton, in *The Early Earth: Physical, Chemical and Biological Development*, edited by C. M. R. Fowler, C. J. Ebinger, and C. J. Hawkesworth, *Geol. Soc. Spec. Publ.*, *199*, 151–181.

Blewett, R. S. (2002), Archaean tectonic processes: A case for horizontal shortening in the North Pilbara Granite-Greenstone Terrane, Western Australia, *Precambrian Res.*, *113*, 87–120.

Bodorkos, S., M. Sandiford, B. R. S. Minty, and R. S. Blewett (2004), A high-resolution, calibrated airborne radiometric dataset applied to the estimation of crustal heat production in the Archaean northern Pilbara Craton, Western Australia, *Precambrian Res.*, *128*, 57–82.

Bouhallier, H., P. Choukroune, and M. Ballevre (1993), Diapirism, bulk inhomogeneous shortening and transcurrent faulting in the Archean Dharwar Craton—The Holenarsipur area, southern India, *Precambrian Res.*, *63*, 43–58.

Brace, W. F., and D. L. Kohlstedt (1980), Limits on lithospheric strength imposed by laboratory experiments, *J. Geophys. Res.*, *85*, 6248–6252.

Buick, R., J. R. Thornett, N. J. McNaughton, J. B. Smith, M. E. Barley, and M. Savage (1995), Record of emergent continental crust ~3.5 billion years ago in the Pilbara craton of Australia, *Nature*, *375*, 574–577.

Burke, K. C. A., J. F. Dewey, and W. S. F. Kidd (1976), Dominance of horizontal movements, arc and microcontinent collisions during the late permobile regimes, in *The Early History of the Earth*, edited by B. F. Windley, pp. 113–129, John Wiley, Hoboken, N. J.

Carter, N. L., and M. C. Tsenn (1987), Flow properties of continental lithosphere, *Tectonophysics*, *136*, 27–63.

Champion, D. C., and R. H. Smithies (2000), The geochemistry of the Yule Granitoid Complex, East Pilbara Granite-Greenstone Terrane: Evidence for early felsic crust, in *Geological Survey of Western Australia Annual Review 1999/2000*, pp. 42–48, Geol. Surv. of West. Aust., Perth.

Chardon, D., P. Choukroune, and M. Jayananda (1996), Strain patterns, décollement and incipient sagducted greenstone terrains in the Archaean Dharwar craton (south India), *J. Struct. Geol.*, *18*, 991–1004.

Chardon, D., P. Choukroune, and M. Jayananda (1998), Sinking of the Dharwar Basin (South India): Implications for Archaean tectonics, *Precambrian Res.*, *91*, 15–39.

Chardon, D., J. J. Peucat, M. Jayananda, P. Choukroune, and C. M. Fanning (2002), Archean granite-greenstone tectonics at Kolar (South India): Interplay of diapirism and bulk inhomogeneous contraction during juvenile magmatic accretion, *Tectonics*, *21*(3), 1016, doi:10.1029/2001TC901032.

Choukroune, P., H. Bouhallier, and N. T. Arndt (1995), Soft lithosphere during periods of Archaean crustal growth or crustal reworking, in *Early Precambrian Processes*, edited by M. P. Coward and A. C. Ries, *Geol. Soc. Spec. Publ.*, *95*, 67–86.

Choukroune, P., J. N. Ludden, D. Chardon, A. J. Calvert, and H. Bouhallier (1997), Archaean crustal growth and tectonic processes: A comparison of the Superior Province, Canada and the Dharwar Craton, India, in *Orogeny Through Time*, edited by J.-P. Burg and M. Ford, *Geol. Soc. Spec. Publ.*, *121*, 63–98.

Collins, W. J. (1989), Polydiapirism of the Archaean Mount Edgar Batholith, Pilbara Block, Western Australia, *Precambrian Res.*, *43*, 41–62.

Collins, W. J. (1993), Melting of Archaean sialic crust under high aH_2O conditions: Genesis of 3300 Ma Na-rich granitoids in the Mount Edgar Batholith, Pilbara Block, Western Australia, *Precambrian Res.*, *60*, 151–174.

Collins, W. J., and M. J. Van Kranendonk (1999), Model for the development of kyanite during the partial convective overturn of Archaean granite-greenstone terranes: The Pilbara Craton, Australia, *J. Metamorph. Geol.*, *17*, 145–156.

Collins, W. J., M. J. Van Kranendonk, and C. Teyssier (1998), Partial convective overturn of Archaean crust in the east Pilbara Craton, Western Australia: Driving mechanisms and tectonic implications, *J. Struct. Geol.*, *20*, 1405–1424.

Cull, J. P. (1982), An appraisal of Australian heat-flow data, *BMR J. Aust. Geol. Geophys.*, *7*, 11–21.

Davies, H. L., and R. G. Warren (1988), Origin of eclogite-bearing, domed, layered metamorphic complexes ("core complexes") in the D'Entrecasteaux Islands, Papua New Guinea, *Tectonics*, *7*, 1–21.

Dawes, P. R., R. H. Smithies, J. Centofanti, and D. C. Podmore (1995), Sunrise Hill unconformity: A newly discovered regional hiatus between Archaean granites and greenstones in the northeastern Pilbara Craton, *Aust. J. Earth Sci.*, *42*, 635–639.

de Bremond d'Ars, J., C. Lécuyer, and B. Reynard (1999), Hydrothermalism and diapirism in the Archean: Gravitational instability constraints, *Tectonophysics*, *304*, 29–39.

de Wit, M. J. (1998), On Archean granites, greenstones, cratons and tectonics: Does the evidence demand a verdict?, *Precambrian Res.*, *91*, 181–226.

DiMarco, M. J., and D. R. Lowe (1989), Stratigraphy and sedimentology of an Early Archaean felsic volcanic sequences, Eastern Pilbara Block, Western Australia, with special reference to the Duffer Formation and implications for crustal evolution, *Precambrian Res.*, *44*, 147–169.

Drummond, B. J. (1988), A review of crust/upper mantle structure in the Precambrian areas of Australia and implications for Precambrian crustal evolution, *Precambrian Res.*, *40/41*, 101–116.

England, P., and M. Bickle (1984), Continental thermal and tectonic regimes during the Archaean, *J. Geol.*, *92*, 353–367.

Eskola, P. E. (1948), The problem of mantled gneiss domes, *Q. J. Geol. Soc. London*, *104*, 461–476.

Green, M. G., P. J. Sylvester, and R. Buick (2000), Growth and recycling of early Archaean continental crust: Geochemical evidence from the Coonterunah and Warrawoona Groups, Pilbara Craton, Australia, *Tectonophysics*, *322*, 69–88.

Haenel, R., L. Rybach, and L. Stegena (1988), *Handbook of Terrestrial Heat-Flow Density Determina-*

tion, with Guidelines and Recommendations of the International Heat Flow Commission, 486 pp., Kluwer Acad., Norwell, Mass.

Hamilton, W. B. (1998), Archaean magmatism and deformation were not products of plate tectonics, *Precambrian Res.*, *91*, 143–179.

Hansen, F. D., and N. L. Carter (1982), Creep of selected crustal rocks at 1000 MPa, *Eos Trans. AGU*, *63*, 437.

Hickman, A. H. (1983), Geology of the Pilbara Block and its environs, *Bull.127*, 268 pp., Geol. Surv. of West. Aust., Perth.

Hickman, A. H. (1984), Archaean diapirism in the Pilbara Block, Western Australia, in *Precambrian Tectonics Illustrated*, edited by A. Kröner and R. Greiling, pp. 113–127, E. Schweizerbart'sche, Stuttgart, Germany.

Hickman, A. H., and S. L. Lipple (1978), Marble Bar W.A. 1:250,000 geological sheet SF 50–8, Geol. Surv. of West. Aust., Perth.

Hill, E. J., S. J. Baldwin, and G. S. Lister (1992), Unroofing of active metamorphic core complexes in the D'Entrecasteaux Islands, Papua New Guinea, *Geology*, *20*, 907–910.

Hill, E. J., S. J. Baldwin, and G. S. Lister (1995), Magmatism as an essential driving force for formation of active metamorphic core complexes in eastern Papua New Guinea, *J. Geophys. Res.*, *100*, 10,441–10,451.

Jaupart, C., and J. C. Mareschal (1999), The thermal structure and thickness of continental roots, *Lithos*, *48*, 93–114.

Jelsma, H. A., P. A. van der Beek, and M. L. Vinyu (1993), Tectonic evolution of the Bindura-Shamva greenstone belt (northern Zimbabwe)—Progressive deformation around diapiric batholiths, *J. Struct. Geol.*, *15*, 163–176.

Kirby, S. H. (1983), Rheology of the lithosphere, *Rev. Geophys.*, *21*, 1458–1487.

Kirby, S. H., and A. K. Kronenberg (1984), Deformation of clinopyroxenite: Evidence for a transition in flow mechanisms and semibrittle behavior, *J. Geophys. Res.*, *89*, 3177–3192.

Kloppenburg, A., S. H. White, and T. E. Zegers (2001), Structural evolution of the Warrawoona Greenstone Belt and adjoining granitoid complexes, Pilbara Craton, Australia: Implications for Archaean tectonic processes, *Precambrian Res.*, *112*, 107–147.

Kröner, A. (1984), Dome structures and basement reactivation in the Pan-African Damara belt of Namibia, in *Precambrian Tectonics Illustrated*, edited by A. Kröner and R. Greiling, pp. 191–206, E. Schweizerbart'sche, Stuttgart, Germany.

Lowe, D. R. (1983), Restricted shallow-water sedimentation of Early Archaean stromatolitic and evaporitic strata of the Strelley Pool Chert, Pilbara Block, Western Australia, *Precambrian Res.*, *19*, 239–283.

MacGregor, A. M. (1951), Some milestones in the Precambrian of southern Rhodesia, *Proc. Geol. Soc. S. Afr.*, *54*, 27–71.

Mareschal, J.-C., and G. F. West (1980), A model for Archaean tectonism. part 2. Numerical models of vertical tectonism in greenstone belts, *Can. J. Earth Sci.*, *17*, 60–71.

Marshak, S. (1999), Deformation style way back when: Thoughts on the contrast between Archaean/Palaeoproterozoic and contemporary orogens, *J. Struct. Geol.*, *21*, 1175–1182.

Marshak, S., F. F. Alkmim, and H. Jordt-Evangelista (1992), Proterozoic crustal extension and the generation of dome-and-keel structure in an Archean granite-greenstone terrane, *Nature*, *357*, 491–493.

Marshak, S., D. Tinkham, F. Alkmim, H. Brueckner, and T. Bornhost (1997), Dome-and-keel provinces formed during Palaeoproterozoic orogenic collapse—Core complexes, diapirs, or neither?: Examples from the Quadrilatero Ferrifero and the Penokean Orogen, *Geology*, *25*, 415–418.

McLennan, S. M., and S. R. Taylor (1996), Heat flow and the chemical composition of continental crust, *J. Geol.*, *104*, 369–377.

McNaughton, N. J., W. Compston, and M. E. Barley (1993), Constraints on the age of the Warrawoona Group, eastern Pilbara Block, Western Australia, *Precambrian Res.*, *60*, 69–98.

Morgan, P. (1985), Crustal radiogenic heat production and the selective survival of ancient continental crust, Proc. Lunar Planet. Sci. Conf. 15th, Part 2, *J. Geophys. Res.*, *90*, C561–C570.

Nelson, D. R. (1998), Compilation of SHRIMP U-Pb zircon geochronology data, 1997, *Geol. Surv. West. Aust. Rec. 1998/2*, 242 pp., Geol. Surv. of West. Aust., Perth.

Nelson, D. R. (1999), Compilation of SHRIMP U-Pb zircon geochronology data, 1998, *Geol. Surv. West. Aust. Rec. 1999/2*, 222 pp., Geol. Surv. of West. Aust., Perth.

Nelson, D. R. (2000), Compilation of geochronology data, 1999, *Geol. Surv. West. Aust. Rec. 2000/2*, 251 pp., Geol. Surv. of West. Aust., Perth.

Nelson, D. R. (2001), Compilation of geochronology data, 2000, *Geol. Surv. West. Aust. Rec. 2001/2*, 205 pp., Geol. Surv. of West. Aust., Perth.

Nelson, D. R. (2002),Compilation of geochronology data, 2001, *Geol. Surv. West. Aust. Rec. 2002/2*, 282 pp., Geol. Surv. of West. Aust., Perth.

Nelson, D. R. (2003), Compilation of geochronology data, 2002, *Geol. Surv. West. Aust. Rec. 2003/2* [CD-ROM], Geol. Surv. of West. Aust., Perth.

Nelson, D. R., A. F. Trendall, and W. Altermann (1999), Chronological correlations between the Pilbara and Kaapvaal cratons, *Precambrian Res.*, *97*, 165–189.

Nyblade, A. A., and H. N. Pollack (1993), A global analysis of heat flow from Precambrian terrains: Implications for the thermal structure of Archaean and Proterozoic lithosphere, *J. Geophys. Res.*, *98*, 12,207–12,218.

Parphenuk, O. I., V. Dechoux, and J. C. Mareschal (1994), Finite-element models of evolution for the Kapuskasing Structural Zone, *Can. J. Earth Sci.*, *31*, 1227–1234.

Pidgeon, R. T. (1984), Geochronological constraints on early volcanic evolution of the Pilbara Block, Western Australia, *Aust. J. Earth Sci.*, *31*, 237–242.

Ranalli, G. (1995), *Rheology of the Earth*, 413 pp., Chapman and Hall, New York.

Richter, F. M. (1985), Models for the Archaean thermal regime, *Earth Planet. Sci. Lett.*, *73*, 350–360.

Ridley, J. R., and J. D. Kramers (1990), The evolution and tectonic consequences of a tonalitic magma layer within Archean continents, *Can. J. Earth Sci.*, *27*, 219–228.

Sandiford, M., and S. McLaren (2002), Tectonic feedback and the ordering of heat producing elements within the continental lithosphere, *Earth Planet. Sci. Lett.*, *204*, 133–150.

Sandiford, M., S. McLaren, and N. Neumann (2002), Long-term thermal consequences of the redistribution of heat-producing elements associated with large-scale granitic complexes, *J. Metamorph. Geol.*, *20*, 87–98.

Shelton, G., and J. Tullis (1981), Experimental flow laws for crustal rocks, *Eos Trans. AGU*, *62*, 396.

Smithies, R. H. (2000), The Archaean tonalite-trondhjemite-granodiorite (TTG) series is not an analogue of Cenozoic adakite, *Earth Planet. Sci. Lett.*, *182*, 115–125.

Thorne, A. M., and A. F. Trendall (2001), The geology of the Fortescue Group, Hamersley Basin, Western Australia, *Bull.144*, 249 pp., Geol. Surv. of West. Aust., Perth.

Thorpe, R. I., A. H. Hickman, D. W. Davis, J. K. Mortensen, and A. F. Trendall (1992a), Constraints to models for Archaean lead evolution from precise zircon U-Pb geochronology for the Marble Bar region, Pilbara Craton, Western Australia, in *The Archaean: Terrains, Processes and Metallogeny*, edited by J. E. Glover and S. E. Ho, *Geol. Dep. Univ. Extension Publ.*, *22*, pp. 395–407, Univ. of West. Aust., Perth.

Thorpe, R. I., A. H. Hickman, D. W. Davis, J. K. Mortensen, and A. F. Trendall (1992b), U-Pb zircon geochronology of Archaean felsic units in the Marble Bar region, Pilbara Craton, Western Australia, *Precambrian Res.*, *56*, 169–189.

Turcotte, D. L., and G. Schubert (1982), *Geodynamics: Applications of Continuum Physics to Geological Problems*, 450 pp., John Wiley, Hoboken, N. J.

van Haaften, W. M., and S. H. White (1998), Evidence of multiphase deformation in the Archaean basal Warrawoona Group in the Marble Bar area, East Pilbara, Western Australia, *Precambrian Res.*, *88*, 53–66.

van Haaften, W. M., and S. H. White (2001), Reply to comment on "Evidence for multiphase deformation in the Archaean basal Warrawoona Group in the Marble Bar area, East Pilbara, Western Australia," *Precambrian Res.*, *105*, 79–84.

van Koolwijk, M. E., K. A. Beintema, S. H. White, and J. R. Wijbrans (2001), Petrogenesis and structures of the basal Warrawoona Group, Marble Bar belt, Pilbara Craton, W.A., in *Fourth International Archaean Symposium 2001 Extended Abstracts*, edited by K. F. Cassidy, J. M. Dunphy and M. J. Van Kranendonk, *AGSO Geosci. Aust. Rec. 2001/37*, pp. 102–103, Geosci. Aust., Canberra.

Van Kranendonk, M. J. (2000), Geology of the North Shaw 1:100,000 sheet, Western Australia, 1:100,000 geological series explanatory notes, Geol. Surv. of West. Aust., Perth.

Van Kranendonk, M. J. (2003), Stratigraphic and tectonic significance of eight local unconformities in the Fortescue Group, Pear Creek Centrocline, Pilbara Craton, Western Australia, in *Geological Survey of Western Australia Annual Review 2001/02*, pp. 70–79, Geol. Surv. of West. Aust., Perth.

Van Kranendonk, M. J., and P. Morant (1998), Revised Archaean stratigraphy for the North Shaw 1:100,000 sheet, Pilbara Craton, in *Geological Survey of Western Australia Annual Review 1997/98*, pp. 55–62, Geol. Surv. of West. Aust., Perth.

Van Kranendonk, M. J., A. H. Hickman, and W. J. Collins (2001a), Comment on "Evidence for multiphase deformation in the Archaean basal Warrawoona Group in the Marble Bar area, East Pilbara, Western Australia", *Precambrian Res.*, *105*, 73–78.

Van Kranendonk, M. J., A. H. Hickman, I. R. Williams, and W. Nijman (2001b), Archaean geology of the East Pilbara Granite-Greenstone Terrane, Western Australia—A field guide, *Geol. Surv. West. Aust. Rec. 2001/9*, 134 pp., Geol. Surv. of West. Aust., Perth.

Van Kranendonk, M. J., A. H. Hickman, R. H. Smithies, D. R. Nelson, and G. Pike (2002), Geology and tectonic evolution of the Archaean North Pilbara Terrain, Pilbara Craton, Western Australia, *Econ. Geol.*, *97*, 695–732.

Van Kranendonk, M. J., W. J. Collins, A. H. Hickman, and M. J. Pawley (2004), Critical tests of vertical versus horizontal tectonic models for the Archaean East Pilbara Granite-Greenstone Terrane, Pilbara Craton, Western Australia, *Precambrian Res.*, in press.

Vitorello, I., and H. N. Pollack (1980), On the variation of continental heat flow with age and the thermal evolution of continents, *J. Geophys. Res.*, *85*, 983–995.

Vlaar, N. J., P. E. van Keken, and A. P. van den Berg (1993), Cooling of the Earth in the Archaean: Consequences of pressure release melting in a hotter mantle, *Earth Planet. Sci. Lett.*, *121*, 1–18.

Weinberg, R. F., and Y. Podladchikov (1994), Diapiric ascent of magmas through power law crust and mantle, *J. Geophys. Res.*, *99*, 9543–9959.

Wellman, P. (2000), Upper crust of the Pilbara Craton, Australia: 3D geometry of a granite-greenstone terrain (2002), *Precambrian Res.*, *104*, 175–186.

West, G. F., and J.-C. Mareschal (1979), A model for Archaean tectonism. part 1. The thermal conditions, *Can. J. Earth Sci.*, *16*, 942–950.

Williams, I. S., and W. J. Collins (1990), Granite-greenstone terranes in the Pilbara Block, Australia, as coeval volcano-plutonic complexes; evidence from U-Pb zircon dating of the Mount Edgar Batholith, *Earth Planet. Sci. Lett.*, *97*, 41–53.

Wingate, M. T. D. (1999), Ion microprobe baddeleyite and zircon ages for Late Archaean mafic dykes of the Pilbara Craton, Western Australia, *Aust. J. Earth Sci.*, *46*, 493–500.

Zegers, T. E., and P. E. van Keken (2001), Middle Archaean continent formation by crustal delamination, *Geology*, *29*, 83–86.

Zegers, T. E., S. E. White, M. de Keijzer, and P. Dirks (1996), Extensional structures during deposition of the 3460 Ma Warrawoona Group in the eastern Pilbara Craton, Western Australia, *Precambrian Res.*, *80*, 89–105.

S. Bodorkos and M. Sandiford, School of Earth Sciences, University of Melbourne, Melbourne, Victoria 3010, Australia. (bodorkos@unimelb.edu.au; mikes@unimelb.edu.au)

M. J. Van Kranendonk, Geological Survey of Western Australia, 100 Plain St., East Perth, Western Australia 6004, Australia. (martin.vankranendonk@doir.wa.gov.au)